Analysis & Sensing

Review
doi.org/10.1002/anse.202400035

Chemistry Europe
European Chemical Societies Publishing

www.analysis-sensing.org

The Promise of Carbon Nano-Onions: Preparation, Characterization and Their Application in Electrochemical Sensing

Hector Daniel Almeida Gonzalez,[a] Janser Hernandez Ojeda,[a] Angel Luis Corcho-Valdés,[b] Ivan Padron-Ramirez,[b] Marina Perez Cruz,[b] Claudia Iriarte-Mesa,*[c, d] Luis Felipe Desdin-Garcia,*[b] Pierangelo Gobbo,*[e] and Manuel Antuch*[e]

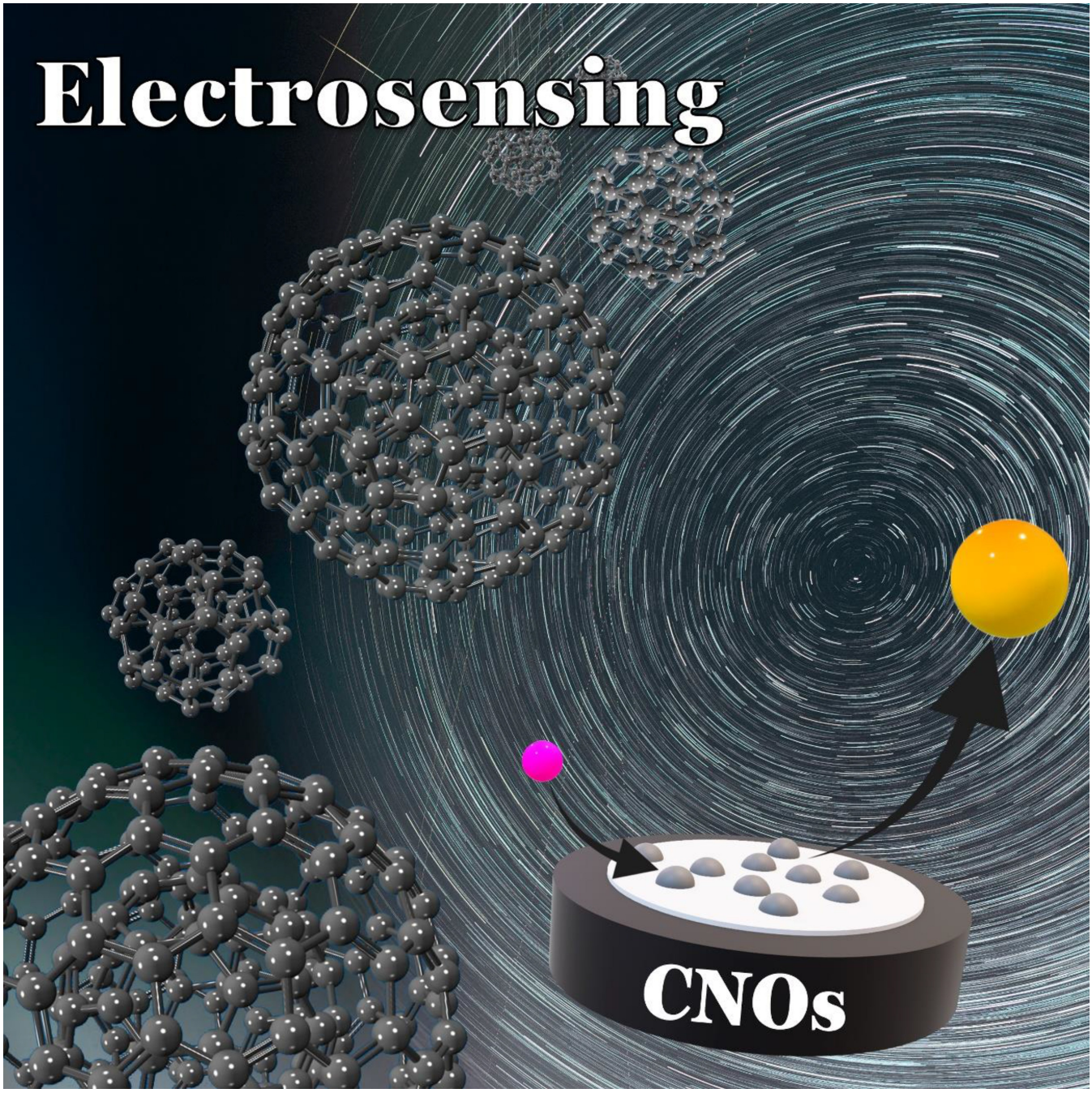

Carbon nano-onions (CNOs) promise to improve the range of applications of carbon materials for electroanalytical applications. In this review, we explore the synthesis, characterization, and electrochemical applications of CNOs. CNO-based sensors present impressive features, including low detection limits in the femtogram per milliliter range, a broad linear detection range spanning up to 7 orders of magnitude, exceptional selectivity, reproducibility, and stability. Synthetic methods and characterization techniques for CNOs were thoroughly examined, shedding light on their pivotal role in biosensing technologies. Comparative analyses with other carbon materials underscore CNOs' competitive performance, either surpassing or matching many counterparts. Despite their relatively recent integration in biosensing applications, CNOs exhibit comparable or superior results concerning other carbon-based materials. Indeed, the incorporation of CNOs into hybrid nanocomposites has shown promising outcomes, indicating a synergistic potential for future advancements in biosensing technologies. Our review provides a broad approach to the application of CNOs to the field, with emphasis on breakthroughs of the last 5 years.

1. Introduction

In recent years, there has been an increase in the study of carbon nano-onions. Although such C allotrope did not receive much attention at their discovery in 1980,[1] they have steadily shown tremendous potential for multiple applications due to their porosity and high surface area, mechanical stability, high conductivity, and biocompatibility.

CNOs are formed by concentric carbon layers made of fullerenes of diverse sizes. In general, CNOs consist of either (i) quasi-spherical nanoparticles or (ii) polyhedral nanoparticles displaying graphitic layers. In addition to typical hexagons, pentagons, and heptagons are also present, as well as holes, that allow the curvature of the carbon network to turn into an onion-like shape. It is well established that the presence of pentagons and heptagons have both a structural contribution to yielding curved structures and also a chemical contribution to the energetic stabilization of giant fullerenes.[2] Moreover, CNOs structure allows the incorporation of different functional groups on the surface, which improves the performance of such materials in applications ranging from biosensing, energy storage,[3] bioimaging,[4] or catalysis.[5–6] The undeniable progress of nanoscience has pushed the use of multiple carbon nanostructures in the field of electroanalytical chemistry. However, CNOs remain the most underexplored among the different carbon nanostructures existing nowadays. This is attributed to the larger attention that has been paid to graphene and carbon nanotubes (CNTs) mainly, but also to carbon nanodiamonds (NDs) and nano-horns, while CNOs are surging as an interesting and promising alternative.

This review focuses on the use of CNOs for electroanalytic applications. Overall, electrochemical sensors allow for identifying changes in electrical potential or current due to selective transformations of specific analytes when in contact with a modified electrode.[7] The unique properties exhibited by nanomaterials such as CNOs promote electron transfer reactions at low potentials, allowing the sensitivity and selectivity of the different electrodes used in biosensing. This is an area that is still under development and increasingly evidences its future projections for the fabrication of more efficient biosensors. Herein, we focus on the different methods of synthesis, characterization, and functionalization of CNOs for their application in sensing, including a critical assessment of the potential and limitations of their use in comparison with other carbon-based nanomaterials.

This review is organized into 6 sections in addition to this introduction. Section 2 provides an overview of the preparation methods of CNOs; section 3 gives a detailed presentation of the different characterization techniques that are typically employed for the characterization of CNOs, and the information that can be retrieved has been carefully tabulated; section 4 provides an insight into the electron transfer properties of CNOs-based electrodes, while section 5 provides a detailed overview of the different architectures for biosensing; finally, section 7 approaches a broad comparison of CNOs in the context of the other carbon nanostructures and their use for electroanalysis. Our work emphasizes the recent progress in the literature, mainly covering the last 5 years, within the period 2020–2024, paying close attention to the latest progress in the field.

[a] *Instituto Superior de Tecnología y Ciencias Aplicadas (InSTEC), Universidad de La Habana, La Habana, Cuba.*
[b] *Centro de Aplicaciones Tecnológicas y Desarrollo Nuclear (CEADEN), Miramar, La Habana, Cuba*
[c] *Department of Functional Materials and Catalysis, Faculty of Chemistry, University of Vienna, Vienna, Austria*
[d] *Vienna Doctoral School in Chemistry (DoSChem), University of Vienna, Vienna, Austria*
[e] *Dipartimento di Scienze Chimiche e Farmaceutiche, Università degli Studi di Trieste, Trieste, TS, Italy*

Correspondence: *Luis Felipe Desdin-Garcia, Centro de Aplicaciones Tecnológicas y Desarrollo Nuclear (CEADEN), Miramar, La Habana C.P. 11300, Cuba.*
Email: luisfelipedesdingarcia@gmail.com

Claudia Iriarte-Mesa, Department of Functional Materials and Catalysis, Faculty of Chemistry, University of Vienna, Währinger Str. 42, 1090 Vienna, Austria.
Email: claudia.iriarte.mesa@univie.ac.at

Pierangelo Gobbo and Manuel Antuch, Dipartimento di Scienze Chimiche e Farmaceutiche, Università degli Studi di Trieste, Via L. Giorgieri 1, 34127 Trieste, TS, Italy.
Email: pierangelo.gobbo@units.it and manuantcubi@yahoo.com

2. Synthesis and Modeling of CNOs

CNOs present a very particular and appealing structure, consisting of concentric walls similar to fullerenes, forming multi-walled motifs (Figure 1), typically.[8] Such carbon allotropes were initially described by Ugarte *et al.*, who synthesized them by treating a sample of CNTs with intense irradiation with an electron beam from a high-resolution electron microscope.[9] Moreover, it has been shown that 200 keV electron irradiation induces structural evolutions in CNOs, producing volume shrinkage and collapsing of the onion-like structure, Y-junctions, and vacancy lines.[10] The effect of electron irradiation in carbon

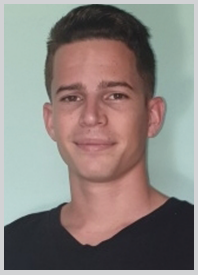

Hector Daniel Almeida Gonzalez is an undergraduate student of Radiochemistry at the Higher Institute of Technologies and Applied Sciences (University of Havana, Cuba). His BSc. work is focused on the photocatalytic properties of heteroatom-doped carbon nanomaterials, under the supervision of Dr. Manuel Antuch. His research interests encompass photocatalysis, nanotechnology, carbon nanomaterials, radiation chemistry, and electrochemistry.

Janser Hernandez Ojeda is an undergraduate student of Radiochemistry at the Higher Institute of Technologies and Applied Sciences (University of Havana, Cuba). He is working at the Center of Technological Applications and Nuclear Development of Cuba, to unveil the interaction between carbon dots and ionizing radiation, under the supervision of Dr. C. Luis Felipe Desdin-Garcia.

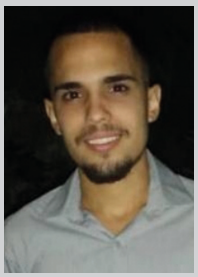

Ivan Padron-Ramirez graduated in Chemistry from the University of Havana, Cuba (2022). He obtained a BSc degree after presenting a thesis on the synthesis of magnetic nanocatalysts for organic reactions. Since January 2023, he started working at Centro de Aplicaciones Tecnológicas y Desarrollo Nuclear in the synthesis and applications of carbon nanostructures. In March 2023, he started pursuing a Master of Science degree in Materials Science under the supervision of Dr. Manuel Antuch and Dr. Luis F. Desdin Garica, related to the determination of gas adsorption at the surface of carbon nano-onions. In May 2023, he participated in the STudent Advanced Research Training (START) at the Joint Institute for Nuclear Physics (JINR), working on the synthesis of nanostructures for cancer therapy.

Marina Perez Cruz obtained a bachelor's degree in chemistry at the University of Havana, Cuba (2023). Her research work dealt with the synthesis of carbon dots for their bioconjugation to vaccines and antibodies. Such work was supervised by Dr. Manuel Antuch, Dr. Luis Felipe Desdín-Garcia, and MSc. Gustavo Gonzaléz Ruiz in the framework of a joint collaboration between the Center for Technological Applications and Nuclear Development (CEADEN) and the Center for Molecular Immunology (CIM). Marina is currently a researcher at CEADEN, where she is working to complete her master's degree in the application of carbon dots for bioimaging applications.

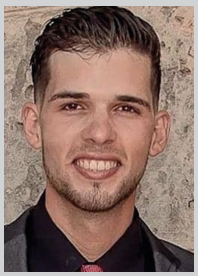

Angel Luis Corcho-Valdes holds a Bachelor of Science degree in Radiochemistry from the Higher Institute of Technologies and Applied Sciences (University of Havana, Cuba). He currently works as a researcher in the Physics Department of the Center for Technological Applications and Nuclear Development (Cuba). His undergraduate thesis focused on the preparation of graphene under the supervision of Dr. Luis Felipe Desdin-Garcia. Currently, he is pursuing a master's degree in Theoretical Chemistry at the Institute of Materials Science and Technology (IMRE-Cuba) under the supervision of Dr. Luis F. Desdin Garcia and Dr. Manuel Antuch. His research interests comprise the preparation of carbon-based materials and the physics of organometallic complexes.

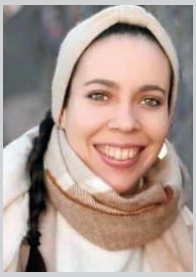

Claudia Iriarte-Mesa received her Bachelor's in Chemistry (2016) and Master's degree (2018) from the University of Havana, Cuba. Her research in the Laboratory of Bioinorganic Chemistry was focused on the conjugation of biomolecules on functional inorganic nanomaterials (i.e., iron oxide nanoparticles, copper sulfide, and gold nanoparticles) for environmental and biomedical applications. In 2019, she joined the Department of Functional Materials and Catalysis of the University of Vienna, Austria, as a research assistant and PhD student under the supervision of Univ.-Prof. Dr. Freddy Kleitz. She earned her PhD in Chemistry on the design of mesoporous silica materials for the oral delivery of peptide drugs and biologics in 2024.

Luis Felipe Desdin-Garcia graduated with a Bachelor's degree in Mathematical Physics from the University of St. Petersburg, Russia. He obtained his M.Sc. from the Unified Institute of Nuclear Research in Dubna and his Ph.D. in Physics from the University of Havana. Currently, he holds the position of Senior Researcher at the Centro de Aplicaciones Tecnológicas y Desarrollo Nuclear in Havana, Cuba, and he serves as a Full Professor at the University of Havana. Additionally, he is an Associate Scientist at the Cuban Academy of Sciences. Dr. Desdin has also held the role of Editor-in-Chief of the journal Nucleus (Cubaenergia) and has served as an expert for National Science Programs and the IAEA. His research focuses on carbon nanomaterials and the interaction of ionizing radiation with nanostructures.

Pierangelo Gobbo received his PhD in 2016 at the University of Western Ontario (Canada). In 2016 he joined the research group of Prof. Stephen Mann, FRS at the University of Bristol (UK) as an NSERC of Canada Postdoctoral Fellow first, and then as an EU Marie Curie Postdoctoral Fellow. In 2019, he established his independent research group at the University of Bristol and started his work on biomimetic tissue-like materials. In 2021, he moved his research group to the University of Trieste (Italy), where he is currently working as an Associate Professor of Organic Chemistry.

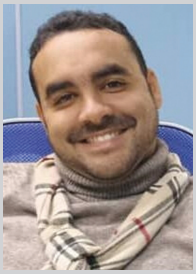

Manuel Antuch is a Marie Skłodowska-Curie Fellow at the University of Trieste studying the incorporation of inorganic semiconductors into artificial protocells. In 2018, he obtained his PhD in Chemistry at the Université Paris-Saclay while working on the photoelectrochemical kinetics of illuminated semiconducting photoelectrodes. He worked as a postdoctoral researcher on inorganic synthesis at École Nationale Supérieure de Techniques Avancées, Institut Polytechnique de Paris (France), as a visiting researcher at the University of Lille (France), and as a Senior Researcher at Centro de Aplicaciones Tecnológicas y Desarrollo Nuclear, in Havana (Cuba).

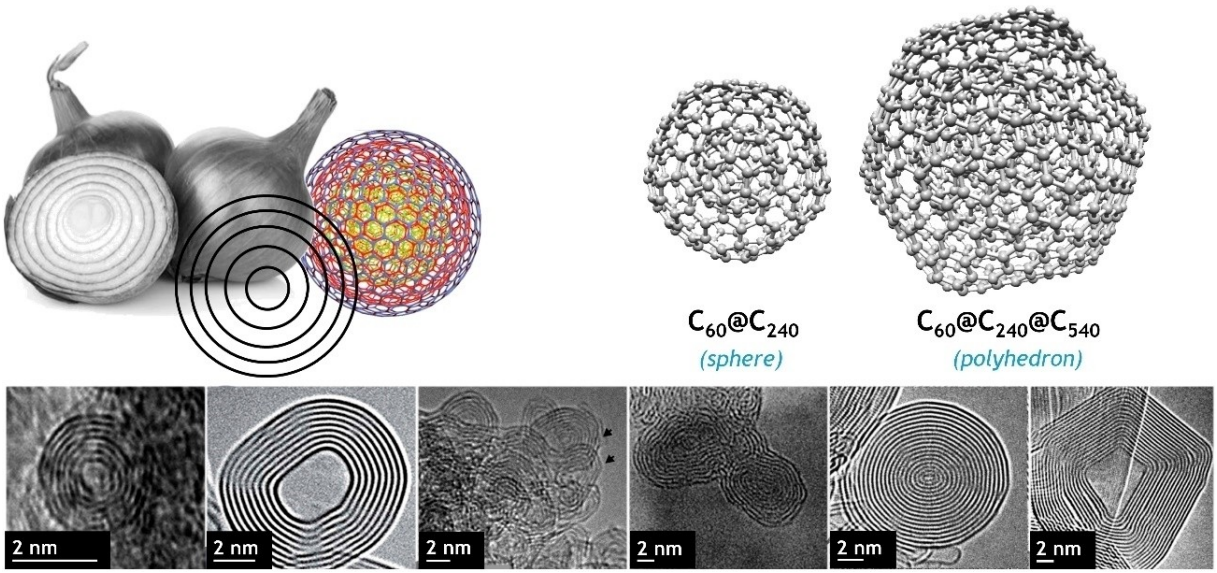

Figure 1. Multi-walled structure of spherical and polyhedral CNOs. Scale bars of the TEM images were adapted and reproduced with permission from refs [13–16]. Copyright © 2007 [13], © 2015 [14], © 2009 [15], and © 2008 [16], WILEY-VCH Verlag GmbH & Co. KGaA, Weinheim.

nanostructures, including CNOs, is well understood, and the reader interested can refer to the work of Banhart *et al.*[11–12]

CNOs also offer the possibility to encapsulate other materials, which confers tremendous flexibility concerning materials design. For example, N-doped CNOs may encapsulate Co nanoparticles by mixing cobalt acetate and $C_{10}H_{15}N_5$ ionic liquid that was heated in an N_2 furnace at different temperatures. Such a material performed well for oxygen reduction and as anode electrodes for Li-ion batteries.[17] Likewise, Ni@CNOs, Fe_3C@CNOs, and $Fe_{0.64}Ni_{0.36}$@CNOs have been obtained after the catalytic decomposition of methane, where nickel, iron, and nickel-iron alloy were seeded for the growth of such nanostructures, that found an excellent application for H_2 storage.[18] CNOs also permit the encapsulation of high-spin ferromagnetic γ-$Fe_{50}Ni_{50}$ nanoparticles obtained using ferrocene, nickelocene, dichlorobenzene, and sulfur as the precursors.[19]

Interestingly, the conductivity of CNOs can be tuned from the experimental conditions set during the synthesis, ranging from 2 to 4 $S\,cm^{-1}$,[20] which is due to the possibility of tuning the concentric multi-shells of CNOs. CNOs are also considered to be more electroactive than other carbon nanostructures, such as nanotubes (*i.e.*, CNTs) and graphene, due to their anisotropic surface and quasi-spherical structures.[21] Furthermore, the kinetics of electron transfer in electrochemical reactions can be modulated by CNO morphology. In this regard, we will analyze the electrochemical reversibility of redox probes when in contact with CNO-based electrode surfaces (section 4). Thus, polyhedral materials (Figure 1) exhibiting more reactive sites (*i.e.*, edge effect) have shown improved performance in electrocatalysis.[22]

Currently, diverse synthetic approaches are implemented to ensure stability and purity of the final product, as well as to improve their electrochemical properties aiming at biosensing. The most common strategies for the synthesis of CNOs include arc discharge, nanodiamond annealing, flame synthesis, hydrothermal synthesis, microwave heating, laser ablation, chemical vapor deposition (CVD), and soft chemistry methods (Figure 2). Each of these synthetic methods will be discussed in more detail below.

2.1. Arc Discharge

Arc discharge is one of the most widely used methods for obtaining carbon nanoparticles worldwide due to its cost-effectiveness and no vacuum requirement during synthesis.[25–30] After arc discharge between two graphite electrodes immersed in water (also known as submerged arc discharge), different nanostructures are formed (Figure 2a). The CNOs obtained present diameters between 5 and 50 nm and show a hydrophobic character, being therefore accumulated at the water surface, which permits their simple separation and purification.[31]

CNOs synthesized by arc discharge have exhibited enhanced electrochemical efficiency in electrochemical sensing (*e.g.*, neurotransmitters). However, their use in aqueous and living systems is limited by the inherent hydrophobic character of the materials obtained. In turn, such CNOs have allowed rapid electron transfer rates, attributed to the rich density of electronic states, close to the formal potential. This effect is closely linked to the presence of functional groups and the near-perfect spherical layered structure.[32]

2.2. Thermal Annealing

Annealing of nanodiamonds leads, in general, to well-structured CNOs (Figure 2b), which are also insoluble in water. However,

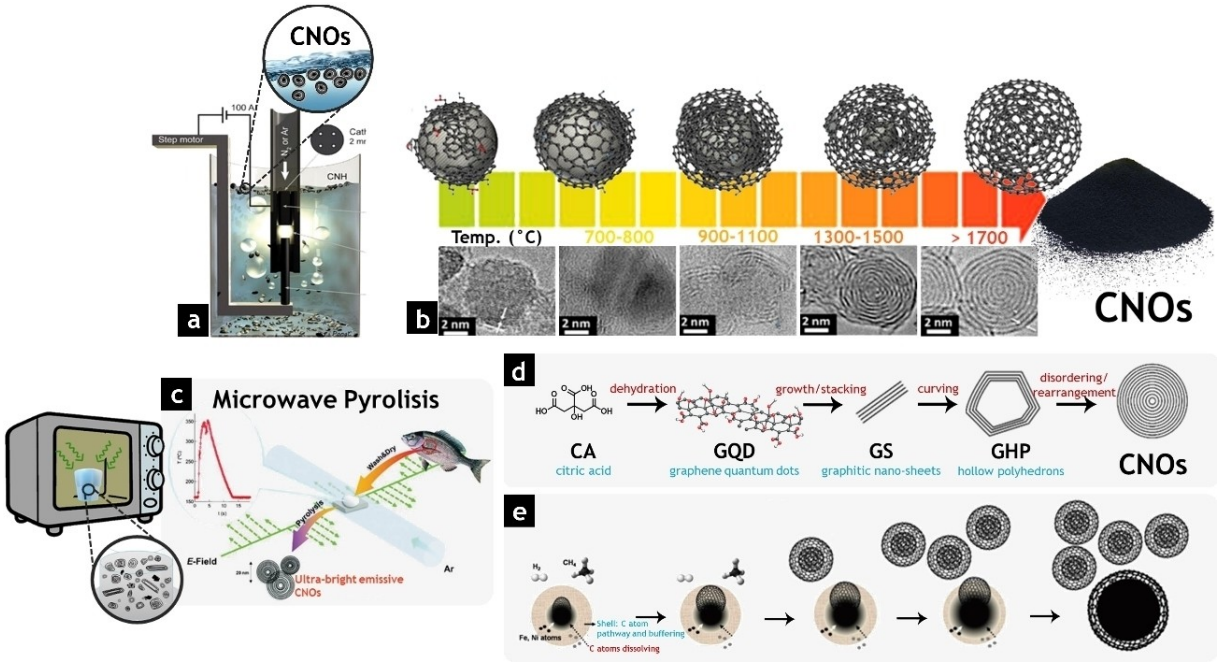

Figure 2. Methods used for the preparation of CNOs. (a) Particles obtained by arc discharge float on the surface due to their hydrophobic character.[21] (b) Transformation of NDs to CNOs through thermal annealing.[23] (c) Green synthesis of CNOs from fish-scale waste.[21] Microwave heating generally conduces to a mixture of particles. (d) Formation of CNOs by hydrothermal synthesis.[24] (e) Representation of the nucleation of graphene layers from inner metal nanoparticles and subsequent growth of CNOs through Chemical Vapor Deposition (CVD).[21] Images were adapted and reproduced with permission from refs. [21,23,24]. Copyright © 2024, [21], Advanced Materials published by Wiley-VCH GmbH. Copyright © 2016, [23], The Royal Society of Chemistry (Creative Commons Attribution 3.0 Unported license, CC BY 3.0, https://creativecommons.org/licenses/by/3.0/). Copyright © 2020, [24], Wiley-VCH GmbH.

this drawback can be overcome by covalent functionalization with biomolecules and non-metallic compounds. Thus, NDs annealing is one of the most widely used synthesis methods for biosensing, rendering CNOs with improved electrochemical performance in comparison to multilayer carbon nanotubes (MWCNTs), graphite nanoflakes (CNFs) and glassy carbon (GC). Furthermore, the resistance of such CNOs to biofouling, as well as their enhanced stability, ensure stable electrode responses to biomolecules.[20]

Radiofrequency Ar/O_2 plasma oxidized CNOs (CNOs-RF)-modified electrodes have demonstrated sensitivity to the relative density of state, contrasting with chemically oxidized CNOs (CNO-OXI)-modified electrodes where electron transfer kinetics were improved by the electrostatic interaction with surface functional groups.[33]

CNOs synthesized from nanodiamond annealing at 1300 °C for 3 h in Ar flow enabled the generation of Pd-CeO_2/CNOs through sol-gel and impregnation methods. Therefore, the combination of Pd nanoparticles with CNOs and CeO_2/CNOs increased the electrochemical performance of the hybrid material in ethanol (Et) sensors.[34]

Nitrogen-doped CNOs (NCNOs) have been synthesized by subjecting a mixture of CNOs with NH_4Cl to temperatures between 300 and 400 °C.[35] NCNOs can also be synthesized directly by thermal annealing of aminated nanodiamonds at temperatures above 1000 °C and reduced pressure.[20, 33–39] The combination of NCNOs with gold nanoparticles (AuNPs) has additionally rendered functional glassy carbon electrodes (GCE) with enhanced electrocatalytic activity for biosensing, as well as high sensitivity, selectivity, and stability for the determination of acetaminophen.[39]

2.3. Pyrolysis

Pyrolysis is an alternative technique well described for the synthesis of CNOs (Figure 2c). As an example, Dhand *et al.* reported the free catalyst synthesis of CNOs by diffusion flames using a mixture of liquefied petroleum gas and air. The final product showed 70 % purity, with densely agglomerated CNOs, diameters between 30 and 40 nm, a high degree of graphitization, and a large specific surface area,[40] which favors their use in energy storage and improves the sensitivity of biosensors fabricated therein.

On the other hand, the combination of gold nanoparticles with CNOs has been frequently evaluated to improve the electrochemical performance of such nanocomposites (Figure 3).

For example, Gowthaman *et al.* reported impregnation of AuNPs on hydrophilic CNOs obtained by flame pyrolysis. The AuNPs/CNOs were self-assembled on the surface of GCE without binder or linker molecules. The obtained hybrid material showed lower onset potential and higher oxidation current than GCE or GC/CNOs. In addition, the AuNPs/CNOs composite offered lower detection limits and high sensitivity, which corresponds with high electronic conductivity.[42]

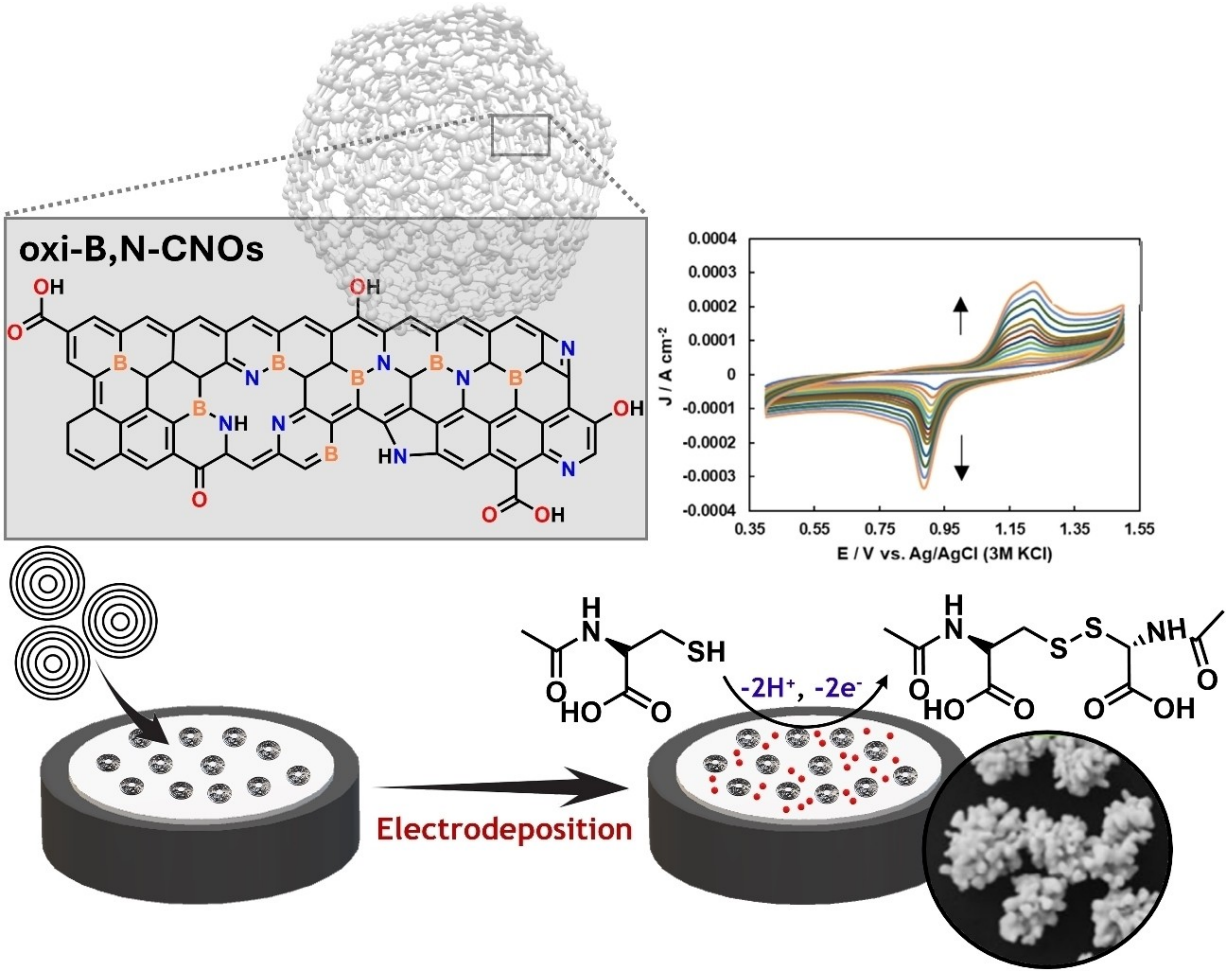

Figure 3. Combination of boron, nitrogen-doped carbon CNOs (oxi-B,N-CNOs) with nanocuboid-shaped gold nanostructures (AuNCBs). The hybrid material (AuNCBs@oxi-B,N-CNOs) was supported on a bare glassy carbon electrode and exhibited enhanced sensitivity toward the inner-sphere oxidative reaction of *N*-acetyl-*L*-cysteine. Images were adapted and reproduced with permission from ref. [41]. Copyright © 2024, Electrochemical Science Advances published by Wiley-VCH GmbH. (Attribution-Noncommercial 4.0 International License, CC BY-NC 4.0, https://creativecommons.org/licenses/by-nc/4.0/).

2.4. Hydrothermal Synthesis

The hydrothermal method implies the formation of dehydrated molecules using lower temperatures in comparison to other methods. Panda *et al.* reported the synthesis of CNOs from mango seeds in a solvent-free autoclave using steam at high pressures and a sustained temperature of 170 °C for 3 h in the oven. These CNOs were used as electrode substrates in the detection of primary amines, secondary amines, and dioxane.[43] The hydrothermal route was also employed by Sang *et al.* to obtain CNOs from citric acid (CA) carbonization at 180 °C. From this study, the authors proposed a synthesis mechanism based on the primary formation of graphene quantum dots from CA dehydration (Figure 2d). Such structures then grow and cluster into graphite nanosheets, which subsequently curve into hollow polyhedrons. These finally transform into CNOs to achieve the minimum interface energy.[24]

2.5. Soft Chemistry

The synthesis methods previously described require high temperatures, high vacancies, and electronic equipment. However, soft chemistry methods have been recently developed to obtain CNOs under mild conditions (Figure 2e).[21, 44] Thus, hydrogenated CNOs (H-CNOs) have been obtained by a simple solvothermal route at low temperatures (100 °C), where graphitic structures were formed at the initial growth stage. In the mechanism proposed by the authors, the released hydrogen interacts with the CNOs, increasing the hydrogenation degree over time.[45] This supported the interpretation that C–Cl and C–H bonds are cleaved by the action of the potassium used to induce $CHCl_3$ reduction during the synthesis, which generates active radicals that assemble to form CNOs.[44]

The oxidation of CNOs by ozonolysis at room temperature has also shown great potential, according to previous studies. Thus, ozonated CNOs (oz-CNOs) have offered potential applications in biosensing attributed to their higher surface area, as

well as increased hydrophilicity and wettability in electrolyte solutions.[46]

2.6. Tools for the Modeling of CNOs

The modeling of CNOs has been carried out using multiple approaches, including Density Functional Theory (DFT) or Molecular Dynamics (MD). Some key examples are provided herein. Hawelek *et al.*[47] studied the transformation of nanodiamonds of around 5 nm into CNOs and constructed structural models for these two structures. The authors used classical molecular dynamics with long-range carbon bond-order potentials to build initial models having pristine nanodiamonds that were annealed at various temperatures (1673 K, 1973 K, and 2273 K) and comprising up to 13 500 C atoms. This work confirmed that the conversion of nanodiamonds into nano onions involves the carbon transformation from sp3 to sp2 hybridization and that the graphitization of the nanodiamonds into quasi-icosahedral giant fullerenes begins from the outer shells of the nanostructure. Another theoretical work concerning the formation of CNOs was provided by Ostroumova *et al.*,[48] where the nucleation of CNOs was followed using MD trajectories and the reactive force field (ReaxFF) interatomic potential. Overall, three main stages were identified: (i) formation and subsequent aggregation of linear molecules, (ii) densification into a droplet-like structure, and (iii) graphitization of the droplet-like structure to form fullerene-type concentric shells. Additionally, Goclon used DFT calculations to determine the structural properties of CNOs and boron-doped CNOs.[49] In such work, the author confirmed that the energy of formation for the systems presenting boron clusters was lower than that for systems with random boron distribution. Furthermore, Goclon *et al.*[50] performed DFT calculations for the evaluation of structural, thermodynamic, and electronic properties of N-doped CNOs, which revealed that pentagons were the most favorable sites for nitrogen doping. Hashmi *et al.*[51] performed high-level electronic structure calculations on double and triple-layered CNOs. They demonstrated that the interactions between the layers in CNOs are dominated by dispersion interactions, supporting the potential applications of CNOs as photosensitizers.

3. Functionalization of CNOs and Synthesis of Hybrid Composites

Carbon nanostructures can be functionalized with materials of organic and inorganic origin or even a combination of both. Particularly noteworthy are combinations involving more than one type of carbon material, which have shown promising results (Figure 4).

For example, Afaque Ansari *et al.*[54] reported the obtaining of a nanocomposite by combining carboxyl-functionalized graphene nanoplatelets (GNPs), CNOs, and chitosan (CS). The hybrid material was used to create an electrochemical aptasensor (Apt) for thrombin detection with an ultra-low limit of detection (LOD, *i.e.*, 8.61 fM).

Pech *et al.*[55] compared the electrochemical performance of CNOs with other carbon-based materials. CNOs showed an open surface with a low electrical resistance, which leads to improved ion migration when compared to MWCNT or carbon black, which was associated with the CNOs morphology,

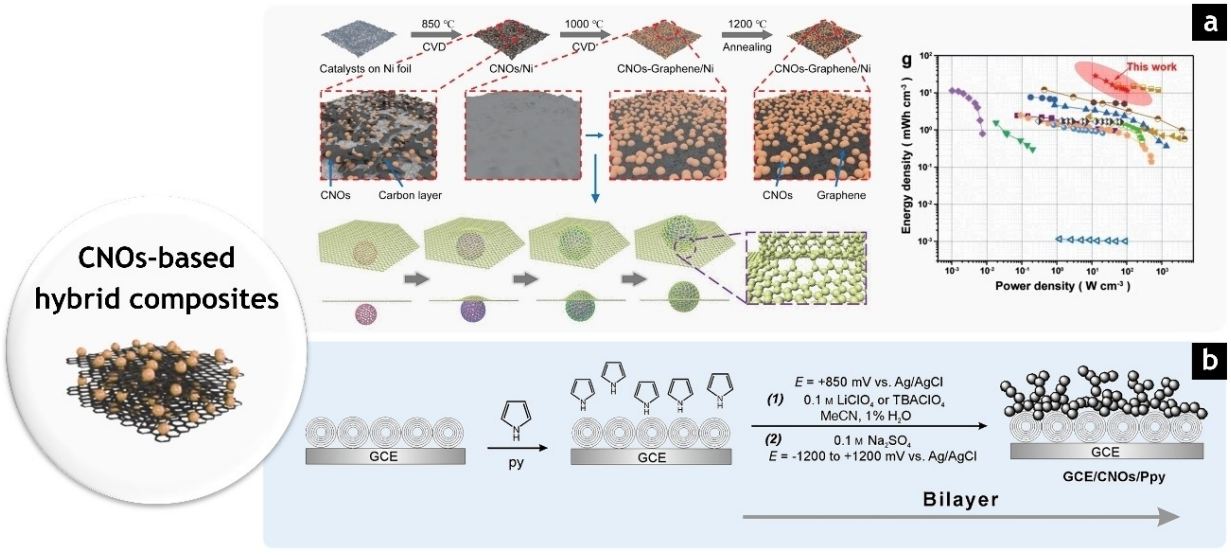

Figure 4. Hybrid composites are obtained by combining CNOs with (a) carbon-based materials or with (b) organic molecules. The CNOs-graphene structure (a) exhibited ultrahigh rate capability, promising for applications in compact filtering units. In this report, the covalent interfacial bonding between CNOs and graphene proved to enable ultrafast ion transportation in the supercapacitor obtained.[52] On the other hand, the combination of CNOs and polypyrrole (Ppy) led to increased specific capacitance of the hybrid device (b), with improved mechanical and electrochemical stabilities.[53] Images were adapted and reproduced with permission from refs. [52,53]. Copyright © 2020, [52], Wiley-VCH GmbH. Copyright © 2015, [53], WILEY-VCH Verlag GmbH & Co. KGaA, Weinheim.

porosity, electronic properties, and their dispersion in aqueous solution.

Bobrowska *et al.*[56] reported a facile method to combine CNOs with zinc oxide (Figure 5). Such a hybrid composite was used for the fabrication of a bulk heterojunction organic solar cell. The incorporation of CNOs allowed the improvement of both power conversion and external quantum efficiencies of the electron transporter layer (CNO/ZnO) when compared to the pristine ZnO.

The electrochemical properties of CNOs have been established as a function of the synthetic procedure that changed the size, shape, and homogeneity of the nano onions of 5 and 6 nm, which corresponds to 6 to 8 graphitic layers. In this context, the annealing at 1650 and 1750 °C showed the highest specific capacitance.[14]

On the other hand, the detection of redox biomolecules such as dopamine (DA), epinephrine (EP), serotonin, uric acid (UA), and ascorbic acid (AA) was tested. CNOs showed superior electrochemical performance, excellent resistance to biofouling, high electrode stability, sensitivity, and selectivity. CNOs have been additionally used for the detection of dopamine mixed with poly(diallyldimethylammonium) (PDDA), with a detection limit of ~10 μM.[57] The improved electrochemical performance of this material was attributed to several features of the CNOs, including morphology, high surface area, porosity, and functional groups present on their surface. Such properties have expanded the range of applications of CNOs in energy storage, sensing, and electrocatalysis (Figure 6).

Sohouli *et al.*[37] reported an electrochemically active surface area (EASA) value of 0.14 cm^2–0.43 cm^2 for CNOs synthesized by the annealing of aminated nanodiamonds. These values are higher than those measured for other carbon nanostructures, such as graphene oxide (0.0686 cm^2–0.3615 cm^2),[64] reduced graphene oxide (0.112 cm^2–0.246 cm^2),[56] and multi-walled carbon nanotubes (0.14 cm^2–0.40 cm^2).[65]

4. Characterization of Modified CNO

The most common techniques used for the evaluation of CNO properties include XPS, Raman Spectroscopy, High-resolution transmission electron microscopy (HRTEM), and X-ray diffraction (XRD).

The efficiency of modified CNOs in analyte biosensing is directly related to their structure. There are then techniques that enable the characterization of the structure, morphology, composition, and electrochemical properties of such materials, directly influencing their performance in sensing and energy storage applications (Figure 7).

4.1. Characterization of CNOs

4.1.1. X-ray Photoelectron Spectroscopy

X-ray Photoelectron Spectroscopy is a non-destructive technique that allows the determination of chemical elements and

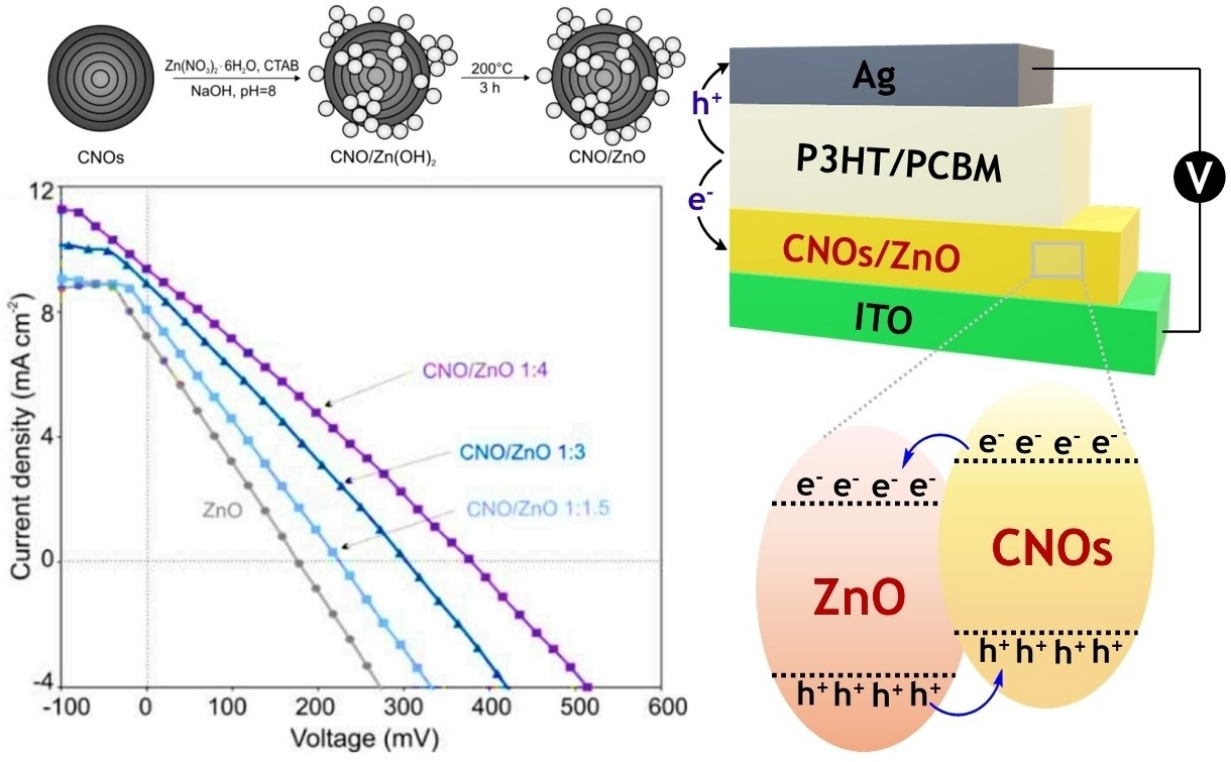

Figure 5. Combination of CNOs with zinc oxide (CNO/ZnO) for the fabrication of organic solar cells. Images were adapted and reproduced with permission from ref. [56]. Copyright © 2019, Wiley-VCH Verlag GmbH & Co. KGaA, Weinheim.

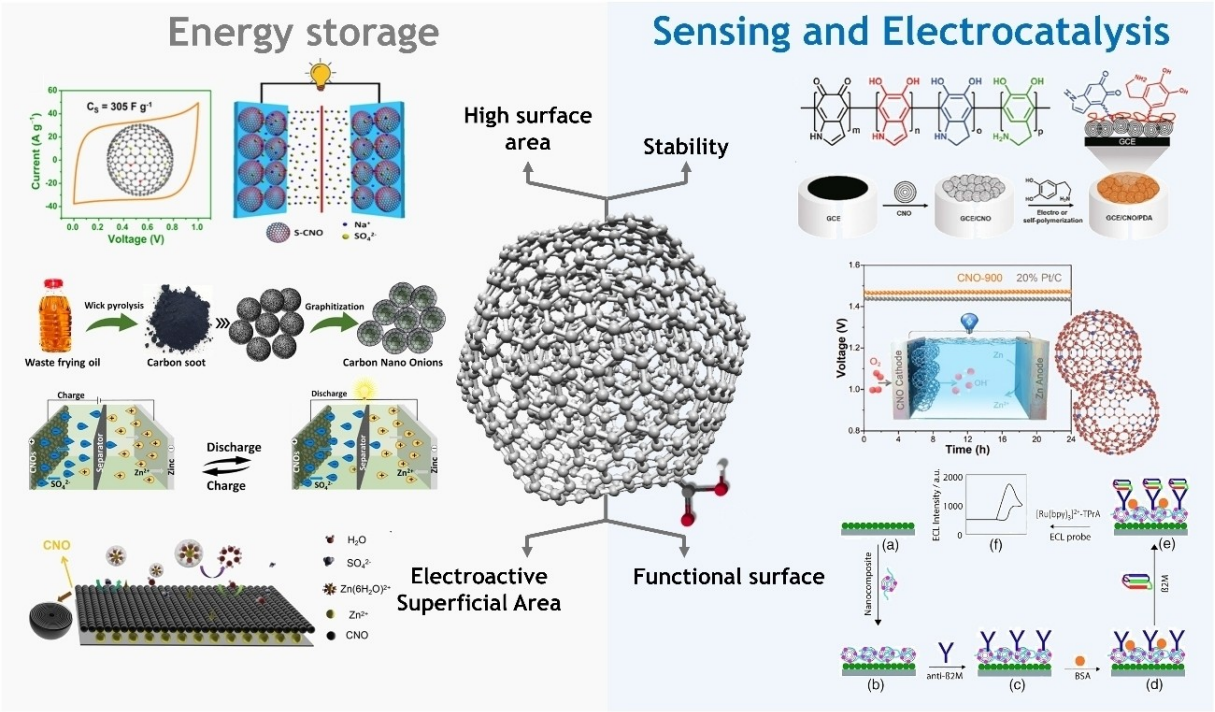

Figure 6. Applications of CNOs in energy storage, sensing, and electrocatalysis. Images were adapted and reproduced with permission from refs. [58–63]. Copyright © 2024, [58], ChemElectroChem published by Wiley-VCH GmbH (Creative Commons CC BY 4.0 license, https://creativecommons.org/licenses/by/4.0/). Copyright © 2023, [59], Elsevier Ltd. Copyright © 2023, [60], Wiley-VCH GmbH. Copyright © 2019, [61], Wiley-VCH Verlag GmbH & Co. KGaA, Weinheim. Copyright © 2023, [62], Wiley-VCH GmbH. Copyright © 2020, [63], Chemical Society located in Taipei & Wiley-VCH Verlag GmbH & Co. KGaA, Weinheim.

their relative abundance via semiquantitative analysis, as well as the chemical environments and oxidation state of the atoms on the electrode surface (~10 nm or 30 atomic layers).[68]

Table 1 summarizes the XPS characteristics of CNOs synthesized by different methods and the respective functional groups present in the samples. It may be observed that moieties such as −OH and −COOH seem to prevail when thermal annealing is used, while in materials synthesized by other methods, C═O and C–O functions are predominant. Concerning other elements analyzed by XPS in samples based on CNOs, we observed that the binding energy of S2p is slightly higher with hydrothermal treatment when compared to pyrolysis, suggesting that S is slightly more oxidized when the latter is used. Moreover, the binding energy of N1s is slightly higher when thermal annealing is used, as opposed to hydrothermal treatment, also suggesting that the oxidation state of N is slightly higher when thermal annealing is employed. Instead, no significant differences are found in O1s values for all synthesis methods compiled in Table 1.

As an example, Zuaznabar-Gardona *et al.*[33] studied by X-ray photoelectron spectroscopy (XPS) the functional groups present in CNOs synthesized by NDs annealing. Thus, the pristine CNOs presented hydroxyl groups (4.3%) and carboxyl groups (3.1%) tethered on the surface, while the oxidized CNOs showed a higher proportion of hydroxyl groups (12.4%) and carboxyl groups (11.5%).

4.1.2. Raman Spectroscopy

Raman Spectroscopy is a technique widely used for the characterization of carbon-based materials. In materials with sp^2 hybridization, two fundamental bands deserve particular attention, *i.e.*, the G- and D-bands (Table 2). The G band is formed from single-resonance in-plane E_{2g} vibrational modes of C–C bonds in the lattice. In turn, the D band appears when defects exist in the lattice (edges, vacancies, C-sp_3, dislocations, among others).

Raman spectroscopy is a technique that permits to distinguish between spherical (SCO) and polyhedral (PCO) CNOs. With this purpose, it is necessary to observe the position and width of the G band. SCO presents a blue-shifted G-band within the range 1570–1575 cm^{-1}. In turn, PCO exhibits a G-band with 2 peaks or a band with a notable broadening. These two distinct peaks are associated with SCO (~1575 cm^{-1}) and graphitic zones (1581 cm^{-1}). The other regions of the Raman spectrum indicate the presence of additional functional groups and decorations on the surface of CNOs.[75]

4.2. High-Resolution Transmission Electron Microscopy

HRTEM allows the evaluation of the nanoparticle size, shape, aggregation state, and dispersity by imaging, as well as the characterization of the nanoparticle distribution in complex matrices. Despite the generally assumed spherical nature of

Review
doi.org/10.1002/anse.202400035
Chemistry Europe
European Chemical Societies Publishing

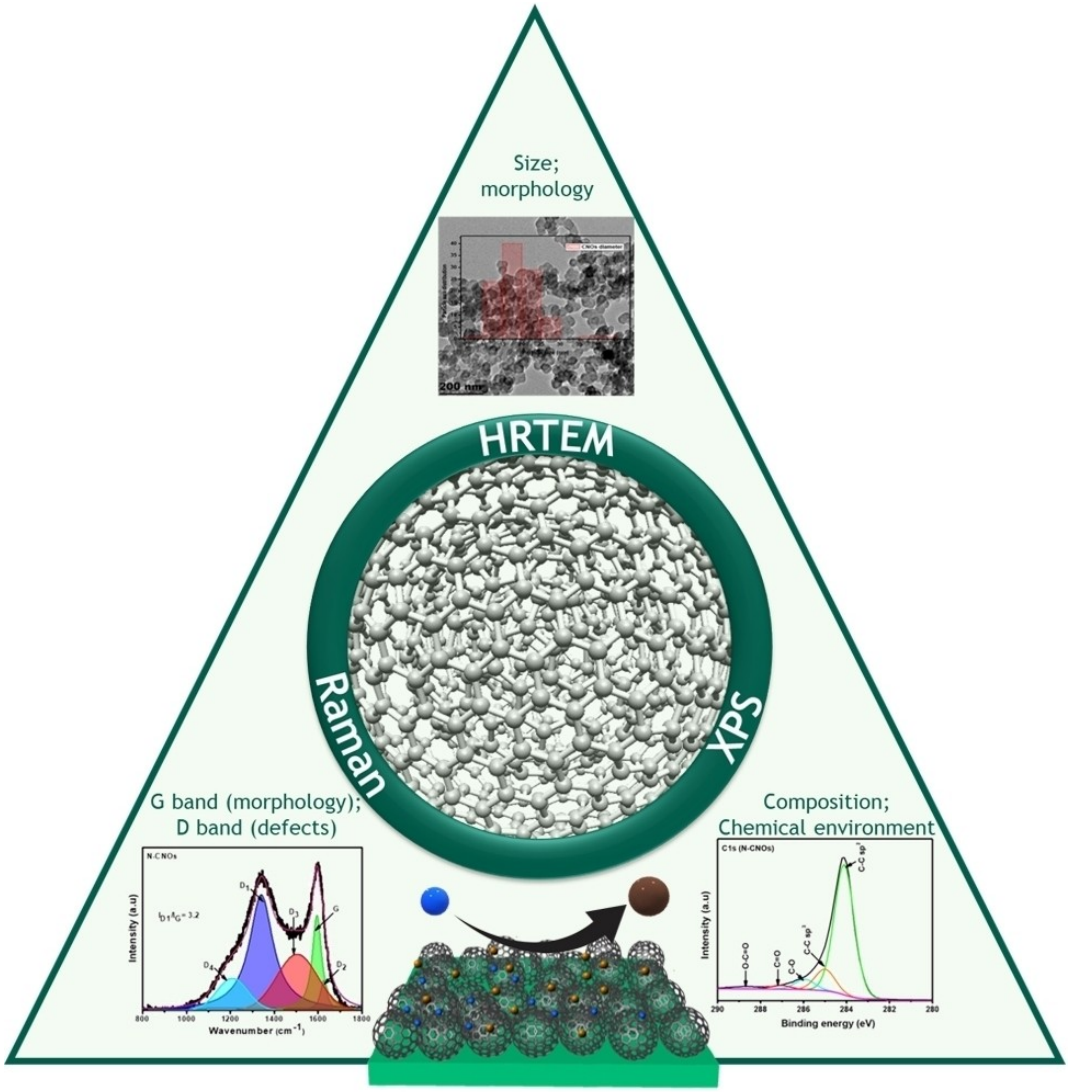

Figure 7. Methods implemented for the characterization of the structure and electrochemical properties of CNOs. The images were adapted and reproduced with permission from ref. [66]. Copyright © 2020, Wiley-VCH GmbH. In this report, Shaku *et al.* described the preparation of nitrogen-doped CNOs to be used as electrode material in supercapacitors. The authors confirmed the successful incorporation of nitrogen into the CNOs lattice, as well as the enhanced electrochemical performance of the doped particles by combining several characterization methods. The graphical representation of the electrocatalytic reaction was adapted from ref. [67]. Copyright © 2022, Licensee MDPI, Basel, Switzerland (Creative Commons Attribution License, CC BY 4.0, https://creativecommons.org/licenses/by/4.0/).

CNOs, different synthetic methodologies yield polyhedral CNOs due to variations in techniques implemented (Table 3). As shown in Table 3, there seems not to be a straightforward connection between the morphology of the CNOs and the procedure implemented for the synthesis. Therefore, thermal annealing, hydrothermal treatment, arc discharge, or pyrolysis can yield spherical CNOs, polyhedral materials, or mixtures. The variables associated with these synthetic methods are complex and not necessarily always controllable, giving rise to this apparent inhomogeneity regarding the morphology obtained. This indicates that further efforts need to be performed in order to truly systematize the preparation of CNOs to obtain desired morphologies and particle sizes.

4.3. X-ray Diffraction

XRD has been the technique of choice for the characterization of crystalline solids. Its main applications are focused on microstructure evaluation based on crystallite size, crystalline phase, crystallographic planes, and layer spacing.[81] Table 4 summarizes the characteristics of XRD patterns of different CNOs obtained by other methods. The signal appearing at around $2\theta = 26°$ and assigned to the [002] set of crystallographic planes is related to pure spherical CNOs whose disordered stacking does not allow the observation of further reflections. On the other hand, polyhedral CNOs also present other reflections that are also typical of graphite.or example, the signals appearing at around $2\theta = 43°$ have been assigned to the [100] or the [101] crystallographic planes.

Table 1. Assignment of the peaks obtained for the different chemical elements in CNO composites.

Material	Preparation method	Peaks	Binding Energy (eV)	Bond	Reference
CNO	Thermal annealing of NDs. Temperature: 1150 °C, Atmosphere: He ~1.1 MPa, for 1 h Cooled to ambient temperature for 1 h	C1s	284.5	C=C	[37]
			285.1	C–C	
		O1s	–	–	
NCNO		C1s	285.3	C=N	
			286.1	C–N	
			286.8	C–O	
			287.5	C=O	
		N1s	398.5	C–N	
			400.3	C–N=C	
		O1s	–	–	
CNO	Hydrothermal treatment. Use autoclave at 170 °C for 3 h Cooled to room temperature	C1s	284.8	C–C	[43]
			286.3	C=C/C–O	
			288.7	O–C=O	
		O1s	531.9	C=O	
			532.5	C–O	
			533.4	O–C=O	
		N1s	397.2	C=N	
			399.6	C–N	
		S2p	168.9	–	
			169.0	–	
			170.1	–	
CNO	Hydrothermal treatment. Use autoclave at 600 °C for 10 h.	C1s	286.0	–	[69]
		S2p	169.0	–	
		Pd3d	336.0	–	
Pristine CNOs	Thermal annealing of NDs	C1s	284.5	C=C	[70]
			285.8	C–C	
			288.2	C=O	
			286.8	C-O	
			290.0	COOH	
			291.3	π-π*	
		O1s	532.0	C=O/COOH	
			533.5	C–O	
			535.0	O–H	
		Si2p	102.3	SiO_2	
			104.4	Si–O-Si	
NeCNOs/ PDDA	Thermal annealing of NDs. Temperature: 1650 °C, Atmosphere: He, for 1 h.	C1s	284.6	C=C	[20]
			285.9	C–OH	
			287.9	C=O	
			290.8	O-C=O	
		N1s	402.9	C-N=C	
		O1s	532.7	–	
CNO	Thermal annealing of NDs	C1s	284.2 and 284.9	C=C	[33]
			285.1	C=C + C–C	
			286.9	C–OH	
			289.0	COOH	
			291.0	π-π*	
CNO-RF	Thermal annealing of NDs. After radio frequency, Ar/O_2 plasma oxidized CNOs	C1s	284.2 and 284.9	C=C	
			286.2	C–OH	

Table 1. continued

Material	Preparation method	Peaks	Binding Energy (eV)	Bond	Reference
			288.1	C═O	
			291.0	π-π*	
CNO-OXI	Thermal annealing of NDs. After chemically oxidized CNO	C1s	284.2 and 284.9	C═C	
			286.2	C–OH	
			288.1	C═O	
			291.0	π-π*	
CNO	Thermal annealing of NDs.	C1s	284.5	C═C	[71]
			285.1	C–C	
			286.5	C–O and C═O	
			287.4	O–C═O	
			290.9	π-π*	
		O1s	532.0	C═O and O–C═O	
Pt@CNO	Pyrolysis. Burning oil on a Cu plate close to a lamp in a wind-free condition	C1s	284.5	C═C	[72]
			285.4	C–C	
			286.3	C–O	
			288.0	C═O	
		Pt4f7/2	71.6	–	
		Pt4f5/2	75.1	–	
CNO	Pyrolysis. Paraffin oil was ignited in a stable, wind-free atmosphere. The structures were captured in an inverted ceramic dish above the flame.	C1s	284.5	C═C	[73]
			285.4	C–C	
			286.5	C–O	
			288.8	C═O	
		O1s	533.0	–	
CNO/MoS_2/Ag	Pyrolysis. Olive oil was burning, and the carbonaceous soot was captured in an inverted beaker over the flame.	Mo3d 5/2	231.3	–	[74]
		Mo3d 3/2	239.5	–	
		S2s	225.4	Mo–S	
		S2p 3/2	161.1	–	
		S2p 1/2	162.2	–	
		Ag3d	367.6	–	
		Ag3d	373.6	–	
		C1s	284.5	C═C	
			285.7	C–C	
			286.9	C–O	
			288.8	C═O	
Au@CNO	Pyrolysis. Inexpensive clarified butter was used as a precursor and pyrolyzed.	Au4f7/2	84.1	Au0	[42]
		Au4f5/2	87.9		
		C1s	284.5	C═C	
			285.7	C–C	
			288.8	C═O/O–C═O	
		O1s	533.0	–	

Table 2. Information obtained by Raman Spectroscopy about the G- and D- bands in CNO composites.

Raman Spectroscopy			
D band (cm^{-1})	G band (cm^{-1})	I_D/I_G ratio	Reference
1340	1577	–	[76]
1346	1575	–	[77]
1320	1598	1.02	[43]
1321	1571	1.23 and 1.49	[70]
1350	1580	–	[20]
1348	1578	0.80 and 0.90	[72]
1345	1588	0.94 and 1.12	[73]
1342	1578	0.79 and 0.89	[42]

Table 3. Diameters and morphology of CNO composites obtained by HRTEM.

Material	Synthetic methodology	Mean diameter (nm)	Morphology	Ref.
CNO	Thermal annealing of NDs	5	Spherical	[76]
CNO	Thermal annealing of NDs. Temperature: 1150 °C, Atmosphere: He~1.1 MPa, for 1 h. Cooled to ambient temperature for 1 h	5	Polyhedral and spherical	[37]
CNO	Arc discharge	5–10	Polyhedral	[77]
CNO	Thermal annealing of NDs	5[a]	Polyhedral[a]	[38]
CNO	Pyrolysis	40–50	Spherical and polyhedral[a]	[78]
CNO	Hydrothermal treatment. Use autoclave at 170 °C for 3 h. Cooled to room temperature	22–32	Spherical	[43]
CNO	Hydrothermal treatment. Use autoclave at 600 °C for 10 h.	20[a]	Polyhedral[a]	[69]
CNO	Thermal annealing of NDs. Temperature: 1650 °C, Atmosphere: He, for 1 h.	6–10	Spherical[a]	[20]
CNO	Thermal annealing of NDs. Atmosphere: He	5–8	Polyhedral[a]	[71]
CNO/Pt	Pyrolysis. Burning oil on a Cu plate close to a lamp in a wind-free condition	27–33	Spherical and polyhedral[a]	[72]
CNO	Pyrolysis. Paraffin oil was ignited in a stable, wind-free atmosphere. The structures were captured in an inverted ceramic dish above the flame.	34	Spherical	[73]
CNO	Carbonization of lycopene with NaOH	30–60	Polyhedral and Spherical	[79]
CNO	Thermal annealing of NDs	15	Spherical	[80]
CNO	Pyrolysis. Inexpensive clarified butter was used as a precursor and pyrolyzed	30	Polyhedral[a]	[42]

[a] This information was not explicitly reported in the original article but was inferred by direct analysis of the corresponding images.

5. Electrochemical Behavior of CNOs

5.1. Cyclic Voltammetry

Cyclic voltammetry (CV) offers qualitative and quantitative information on redox reactions (*e.g.*, the kinetics of heterogeneous electron transfer reactions, the thermodynamics of redox processes, and the coupled chemical reactions or adsorption processes). The peak-to-peak separation (ΔE_p) in cyclic voltammetry gives a direct measurement of the kinetics of electron transfer of modified electrodes when put in contact with a redox probe, such as the hexacyanoferrate ion. In the case of a diffusion-controlled process, the $\Delta E_p = 59/n$ mV, where n is the number of electrons involved in the redox reaction.[83–84] An increase in ΔE_p indicates sluggish electron transfer kinetics. An analysis of Table 5 suggests that CNOs and CNO-OXI exhibiting ΔE_p values of 89 mV and 70 mV, respectively, are excellent regarding the kinetics of charge transfer at the electrode surfaces. This makes them appealing as platforms for electroanalytical applications. However, further modification of CNOs with other species or polymers has a detrimental effect on electron transfer kinetics, as expressed by the increased ΔEp. Anyhow, such a decrease in electron transfer kinetics upon CNO modification or insertion within complex composites is to be expected and does not hinder the applications of these carbon nanostructures for electroanalysis, as will be presented in the following sections.

Table 4. Crystallographic information obtained by XRD of different composites of CNOs.

Material	Synthetic methodology	XRD reflection (2θ (°))	Crystallographic plane	References
CNO	Arc discharge Temperature: Room temperature. Atmosphere: Nitrogen	26	[002]	[77]
		44	[101]	
	Pyrolysis Mixture through ultrasonication	25	[002]	[78]
		40	[100]	
	Hydrothermal treatment Use autoclave at 170 °C for 3 h. Cooled to room temperature	25.5	[002]	[43]
	Hydrothermal treatment Use autoclave at 600 °C for 10 h.	26	[002]	[69]
	Pyrolysis. Burning oil on a Cu plate close to a lamp in a wind-free condition	25.1	[002]	[72]
		43	[100]	
		44	[101]	
	Thermal annealing of NDs	22.8	[002]	[82]
		43.3	[100]	
	Pyrolysis Use autoclave at 200 °C for 24 h. Cooled to room temperature	25	[002]	[74]
	Thermal annealing of NDs. Temperature: 1150 °C, Atmosphere: He~1.1 MPa, for 1 h. Cooled to ambient temperature for 1 h	24.3	[002]	[39]
		44	[101]	
	Pyrolysis Inexpensive clarified butter was used as a precursor and pyrolyzed	24.5	[002]	[42]

5.2. Electrochemical Behavior Observed by Electrochemical Impedance Spectroscopy

Electrochemical impedance spectroscopy consists of applying a sinusoidal potential perturbation of variable frequency to the electrode under study and recording the sinusoidal current that appears as a response to the potential perturbation. By measuring small changes in the electrode | electrolyte interface, electrochemical impedance spectroscopy (EIS) is becoming a powerful technique to understand the electrochemical mechanism related to bio-recognition events, *e.g.*, the antigen-antibody, recognition of specific proteins, receptors identification, nucleic acids, or whole cells.[37, 86–87] The use of EIS in electroanalysis is frequent and typically deals with the correlation of the charge transfer resistance with the concentration of the target analyte. Table 6 shows a summary of EIS measurements for electrodes based on CNOs.

6. Electroanalytical Applications

For electrochemical analysis, it is essential to selectively detect a target analyte in the presence of interfering molecules with high sensitivity. In this sense, CNOs constitute an excellent platform for biosensing primarily due to their large surface area, which allows for more significant adsorption of biomolecules. Furthermore, the high conductivity of CNOs privileges the detection of electrochemical changes that occur when specific molecules, such as dopamine, are joined together.[69] The origin of the metal-like behavior in CNOs has been recently addressed via the calculation of systems with 7 concentric shells and beyond 13,000 atoms. The main conclusion taken was that concentric structures of fullerene-like shells display semiconducting behavior. In contrast, the random breaking of the shells confers metallic conductivity to the CNOs and is thus essential for the reproduction of experiments.[88]

Another interesting issue to account for is the difference in reactivity that may exist according to the different defects present in carbon nanostructures. In particular, the specific reactivity of pentagons has been assessed in pentagon-defect-rich carbon nanomaterial and compared to C_{60} in the particular case of electrochemical oxygen reduction.[89] The authors attributed the superior oxygen reduction ability to the high charge density located at the pentagon rings and the higher affinity for O_2 adsorption. The key conclusion was that the high density of pentagons was a determinant in the superior electrocatalytic activity. A different example aiming to explain the reactivity of curved carbon nanostructures towards the H atom and methyl radical has been reported.[90] The authors realized that reaction heat depended linearly on the strain and curvature of the carbon surface, which provides clues on the different reactivity that curved carbon structures might show. However, to the best of our knowledge, such a detailed study on the reactivity of CNOs with regard to surface defects (pentagons vs. hexagons vs. heptagons), surface strain, the effect of inner layers of fullerene-like shells, or the specifics of

Table 5. Electrochemical information by CV for different composites of CNO.

Material	Electrolyte	ΔEp (mV) (scan rate at which ΔEp was determined)	Range of scan rates explored (mV/s)	Ref.
PANI/CNO	5 mM $Fe(CN)_6^{3-/4-}$ and 0.1 M PBS	140 (50 mV/s)	40–300	[76]
Screen-printed carbon electrode (SPCE)/ NCNO/AuNPs/Apt/ S. aureus	1 mM $Fe(CN)_6^{3-/4-}$ and 0.1 M KCl	135 (100 mV/s)	50	[37]
CNO	5 mM $Fe(CN)_6^{3-/4-}$ and 0.1 M KCl	89 (50 mV/s)	50	[77]
AuNPs/Single-walled carbon nanotube (SWCNTs)/CNO/CS	1 mM $Fe(CN)_6^{3-/4-}$ and 0.1 M KCl	149 (100 mV/s)	100	[38]
ZnO/CNO	$Fe(CN)_6^{3-/4-}$ and 0.1 M NaOH	–	50	[78]
CNO/GRT	1 mM FcMeOH and PBS pH = 7,4	160 (50 mV/s)	10–200	[70]
CNO-CNF	0.1 M $Fe(CN)_6^{3-/4-}$ and 0.1 M PBS	500 (50 mV/s)	10–175	[85]
CNO-OXI	1 mM $Fe(CN)_6^{3-/4-}$ and 0.2 M $HClO_4$	70 (100 mV/s)	100	[33]
CNOs/Ñafian	10 mM $Fe(CN)_6^{3-/4-}$ and 0.1 M KCl	329 (20 mV/s)	20	[72]
Pt@CNOs	10 mM $Fe(CN)_6^{3-/4-}$ and 0.01 M PBS	105 (10 – 20 – 50 – 100 mV/s)	10–100	
NCNO/AuNP	5 mM $Fe(CN)_6^{3-/4-}$ and 0.1 M KCl	250 (50 mV/s)	10–500	[39]
GPS/CNOs/CS	5 mM $Fe(CN)_6^{3-/4-}$ and 0.1 M KCl	100 (100 mV/s)	20–100	[54]
s-OLCs (onion-like carbon)	$Fe(CN)_6^{3-/4-}$ and 1 M H_2SO_4	200 (10 – 50 – 100 – 500 – 1000 50 mV/s)	10–1000	[73]
AgNDs/CNOs/GCE	5 mM $Fe(CN)_6^{3-/4-}$ and 0.1 M KCl	–	100	[82]
SPCE/CNO/MoS 2 /Ag dendrites	$Fe(CN)_6^{3-/4-}$ and 0.1 M KCl	100 (—)	–	[74]
Au/Apt/ox-CNOs/Methyleneblue(MB)	1 mM $Fe(CN)_6^{3-/4-}$ and 1 M H_2SO_4	100 (50 mV/s)	100	[39]
Au@CNO	2 mM $Fe(CN)_6^{3-/4-}$ and 0.2 M KCl	140 (50 mV/s)	10–100	[42]

Table 6. Electron transfer resistance values by EIS for different composites of CNOs.

Material	Electrolyte	Frecuency range (kHz)	Charge transfer resistance (R_{ct})	Ref.
Au/Apt/ox-CNOs/Methylene blue	1 mM $Fe(CN)_6^{3-/4-}$ and 0.1 M KCl	-	200 Ω	[37]
CNO/GCE	5 mM $Fe(CN)_6^{3-/4-}$ and 0.1 M KCl	-	327.9 Ω	[77]
$Pd/SO_3H/CNO$	5 mM $Fe(CN)_6^{3-/4-}$ and 0.1 M KCl	$5 M. 10^{-5}$–82.500	-	[69]
CNO-Carbon nanofibers	0.1 M $Fe(CN)_6^{3-/4-}$ and 0.1 M PBS	10^{-5}–100	17.6 Ω	[85]
CNO-OXI	1 mM $Fe(CN)_6^{3-/4-}$ and 0.2 M $HClO_4$	0.4 (constant frequency by scanning the DC potential from −0.5 to 0.9 V)	-	[33]
NCNO/AuNP	5 mM $Fe(CN)_6^{3-/4-}$ and 0.1 M KCl	–	18 Ω	[39]
s-CNOs	$Fe(CN)_6^{3-/4-}$ and 1 M H_2SO_4	10^{-3}–100	13.1 Ω	[73]
CNOs	5 mM $Fe(CN)_6^{3-/4-}$ and 0.1 M KCl	–	917.6 Ω	[82]
CNO/MoS_2 /Ag dendrites	$Fe(CN)_6^{3-/4-}$ and 0.1 M KCl	0.1–100	0.4	[74]
Au@CNO	2 mM $Fe(CN)_6^{3-/4-}$ and 0.2 M KCl	10^{-5}–100	2290 Ω	[42]

analyte adsorption, is missing in the literature and remains a gap to be filled by theoretical and experimental means.

Another critical issue is related to the chemical stability of CNOs to achieve long-term durability.[37] The functional groups present on the surface of the nanomaterial could enhance the analytical signal due to their affinity for the analyte and could also contribute to the design of hybrid composites.

When sensing biomolecules, a high surface area results in greater exposure to the target molecule, which increases the desired analytical signal and the detection capability even at low concentrations. This feature is also essential for the immobilization of biomolecules, rendering improved sensitivity and selectivity due to efficient interactions with the receptors. Higher porosity is additionally desired to accommodate a larger volume of functional materials or molecules, which could improve the analytical parameters of these biosensors.[91]

Investigations utilizing palladium-decorated CNOs for dopamine detection disclosed a LOD value of 2.44 μM and a linear range of 10–400 μM for dopamine (DA). The heightened electrocatalytic performance towards DA was ascribed to the high active surface area, conductivity of CNOs, and palladium's exceptional electrocatalytic properties.[69]

Mohapatra *et al.* explored CNOs as an electrochemical sensor by covalently linking the glucose oxidase enzyme via carbodiimide chemistry. This approach yielded a sensitivity of 26.5 $\mu A\,mM^{-1}\,cm^{-2}$ with a linear response spanning 1–10 mM glucose (Glu). Such material was decorated with platinum nanoparticles to enhance the catalytic performance and enzyme-free nature of the CNOs. The resultant sensor containing Pt-decorated CNOs exhibited a superior sensitivity of 21.6 $\mu A\,mM^{-1}\,cm^{-2}$ with a linear response in the range of 2–28 mM glucose.[72]

In previous studies, the possibilities of utilizing aptamers for detecting specific drugs like epirubicin have been showcased, albeit with reported selectivity not being particularly high.[36] The use of CNOs has provided, instead, an effective solution for this issue: Sohouli *et al.* demonstrated the selectivity of gold electrodes coupled with a thiolated aptamer, which was reinforced with CNOs and methylene blue. The synthesis of the aptasensor was carried out by keeping the gold electrode in the aptamer solution and then in the CNO solution for a certain time under pH = 7.4. In addition to the positive effect on selectivity, the conductivity was increased with a marked synergistic effect.[37]

Recently, biosensors based on the inhibition of peroxidase activity have been constructed from CNOs synthesized by annealing nanodiamonds. This material was obtained by NDs annealing and further oxidized with HNO_3/H_2SO_4 (1 : 3 ratio). The carboxylated CNOs were finally functionalized with maleimide-activated peroxidase. The biosensors obtained exhibited excellent electron transfer properties, stability, and repeatability.[38]

The oxidation levels of the CNOs can influence the biosensor's sensitivity. Regarding the detection of H_2O_2, a correlation was observed where sensitivity heightened with increasing CNO oxidation levels. In contrast, for detecting dopamine, uric acid, and ascorbic acid, non-oxidized CNOs demonstrated superior sensitivity and peak resolution.[33]

Ogada *et al.* reported the use of a composite based on Pd-CeO_2/CNOs nanocrystals for ethanol detection. The Pd-CeO_2/CNOs provided excellent sensitivity (0.00024 mA/mM) and detection limit (8.7 mM), attributed to the porosity of CNOs. In turn, CeO_2 allows to increase the adsorption of OH^- on the active sites of the surfaces.[34]

Furthermore, CNOs have been widely studied as electrochemical sensors to determine biomolecular interactions. In this regard, Rui An *et al.* carried out a study for the simultaneous detection of dopamine (DA), uric acid (UA), L-tryptophan (Trp), and theophylline (TP) by applying a differential pulse voltammetry technique. This allowed to evaluate the electrocatalytic activity of a sensor composed of a GCE modified with CNOs (CNOs/GCE).[77] This sensor exhibited detection limits, surpassing other electrodes with values of 0.0039 μM, 0.0087 μM, 0.18 μM, and 0.35 μM for DA, UA, Trp, and TP, respectively.[77] The anti-interference capacity of CNOs/GCE was evaluated using a mixture of interfering species like Cl^-, SO_4^{2-}, K^+, Na^+, glycine (Gly), L-lysine, L-valine, adenine (Ad) and ascorbic acid (AA). The results indicated the ability of the CNOs/GCE to detect the studied system selectively. Likewise, CNOs/GCE demonstrated good stability through a 30-day study and showed good reproducibility and repeatability in the simultaneous determination of DA, UA, Trp, and TP. Hence, this study revealed the potential of CNO-based sensors to be used for accurate sample detection.[77]

In a recent study, a palladium-decorated CNO (Pd/CNO) was developed as an electrochemical catalyst for detecting DA.[69] This Pd/SO_3H/CNO biosensor achieved a sensitivity of 1.93 ± 0.14 $\mu A/\mu M{\cdot}cm^2$ within a linear range from 10 to 400 μM DA. The sensor demonstrated a detection limit of 2.44 μM, notably smaller than other reported findings. The selectivity of the sensor was determined using interference species such as ascorbic acid, uric acid, glucose, and hydrogen peroxide. The results confirmed a high selectivity. Also, a 22-day test showed the good stability of the Pd/SO_3H/CNO.[69]

Various reports deal with the electrochemical determination of glucose to develop sensors that do not involve the use of the glucose oxidase enzyme.[72, 78–79] Ankita Sharma *et al.*[78] described the enzyme-less biosensing property of CNOs modified with zinc oxide nanocomposite (ZnO/CNO). Such a sensor was obtained by coating a GCE with the ZnO/CNO nanocomposite. Glucose detection was significantly improved due to the presence of both ZnO and CNOs, showing a sensitive value of 606.64 $\mu A/mM\,cm^2$. Various biomolecules, including ascorbic acid, citric acid, lactic acid, ethanol, glycerol, and urea, were utilized to assess the anti-interference capability of ZnO/CNO nanocomposites for glucose detection. Results highlighted the sensor's effectiveness in isolating the analyte molecule from interfering substances. Additionally, the ZnO/CNO nanocomposite exhibited satisfactory repeatability during a 40-day trial. Altough stability could potentially be improved, it still outperformed other sensors in glucose sensing.[78]

Incorporating heteroatoms has been found to enhance the electrocatalytic and electrochemical functionality of CNOs.[39, 92]

A recent study focused on the individual and simultaneous determination of dihydroxybenzene isomers (*i.e.*, Hydroquinone (HQ), Catechol (CC), resorcinol (RS)) through nitrogen-doped CNOs (NCNOs) development.[92] This sensor showcased exceptional sensitivity and minimal detection limits, outperforming other sensors. Stability and repeatability assessments of the NCNO electrode confirmed its reliability for the simultaneous detection of such isomers, demonstrating high sensitivity and low detection limits.[92]

On the other hand, AuNPs stand out among various nanoparticles due to their innovative ability to interact with biological systems. Thus, multiple studies have used AuNPs to modify CNOs for sensing applications.[39, 93] A recently published report addressed the determination of environmental pollutant hydrazine (HZ) using CNOs decorated with AuNPs (Au@CNOs) deposited on the surface of an electrode.[42] The Au@CNOs exhibited a larger active area for electrochemical reactions and excellent electronic conductivity, attributed to an exceptionally low detection limit of 12 nM, along with an improved sensitivity of 485.7 μA/mM cm^2.[42] Au@CNOs additionally exhibited selectivity towards HZ in the presence of interferences such as atrazine (Atr), H_2O_2, RS, oxalic acid, and urea, as well as long-term stability and reproducible performance.[42]

The detection of acetaminophen (AMP) has been recently reported by using nitrogen-doped CNOs modified with gold nanoparticles.[39] This nanocomposite-based sensor allowed AMP detection in the range of 25 nM to 35 μM, showcasing a remarkable detection limit of 9 nM.

Table 7 shows a summary of different electrochemical sensors reported in recent articles and their efficiency for biomolecule detection. Overall, these studies demonstrate the efficacy of CNOs as biosensors in detecting a wide range of analytes.

7. Comparison with Other Carbon Nanostructures

For years, the use of nanostructures[94] and, in particular, carbon nanostructures, such as graphene and CNTs,[95] have been present in biosensor research and continue to be highly useful in this field. However, the recent exploration of the potential of CNOs in such applications has allowed these nanostructures to stand out compared to others despite the relatively short time they have been in use. Table 8 presents some recent works on carbon materials biosensors, highlighting specific parameters that can define the potential of each material.

A combined analysis of Tables 7 and 8 shows that carbon nanostructures, in general, are very useful for electroanalysis, given the large variety of target analytes that can be determined using electrochemical techniques. It is essential to highlight that when CNOs are used, improved LODs are achieved, reaching the range of the nM. The use of these sensors is appropriate for accurate sample analyses, given their stability and robustness. Certainly, CNOs are offering today a very flexible platform with fast electron transfer kinetics and chemical stability, permitting the determination of an extensive range of different analytes via electroanalysis. The breath of molecules and their tremendous variety, as expressed by Table 7, place CNOs in a privileged position as nanomaterials very well adapted for electrochemical sensing.

7.1. Limits of Detection

CNOs have been successfully utilized to create biosensing devices with very low limits of detection. For instance, Huang *et al.*[80] developed a solid/liquid two-phase dual-output biosensor for detecting ovarian cancer biomarkers with an LOD of 3.3 fg mL^{-1}. This remarkably low LOD demonstrates the efficiency of CNOs. The detection limits achieved from studies involving CNTs and graphene stand out. For instance, Cui *et al.*[102] detected bacterial endotoxin with an LOD of 4.6 fg mL^{-1} using CNTs, while graphene-based devices in Dou *et al.*'s work[106] obtained a detection limit of 33.6 fg/mL. Despite these detection limits being close, they are less precise than those achieved with CNOs, as mentioned earlier. Noteworthy results have been obtained in biosensors using CDs[113] and nanodiamonds,[97] but their LODs are not as low. There are some works with even lower LODs. For example, Chen *et al.*[108] fabricated a graphene-based material modified with chitosan that was included in a field-effect transistor biosensor for ultrasensitive procalcitonin with a LOD of 0.82 ag/mL. Although surpassing the LOD obtained with CNOs, other parameters have been highlighted in which they excel.

7.2. Linear Detection Range

There is a wide range of devices based on CNOs that cover linear detection ranges from tens to several orders of magnitude.[37, 42, 54, 69, 74, 77, 80, 82] The work of Gowthaman *et al.*[42] should be highlighted since the Au@CNO-based device achieved a linear detection range from 0.05 to 1000 μM. These values were reached due to the extensive surface area of the particles used and their high electrical conductivity. Similarly, biosensors with a broad detection range based on CDs have been obtained,[110–111, 114] with particles noted for their improved optical and electrical properties and extensive surface area. CNTs also exhibit similar properties and based on these, Ma *et al.*[100] constructed a triple-aptamer tetrahedral DNA nanostructures-based carbon-nanotube-array transistor biosensor for detecting the SARS-CoV-2 virus antigen not only with a very low LOD but also with a broad linear detection range of up to eight orders of magnitude. The ranges achieved by devices based on graphene are notable as well.[108–109] In the realm of diamond biosensors,[96–97] the recent detection ranges have yet to match those achieved by other carbon materials, typically spanning 5–8 orders of magnitude, as seen in specific CNOs-based devices.[80]

Table 7. Application of CNOs in biosensing.

System	Electrodes	Target analyte	Electrolyte	Detection method	Detection limit	Linear Range	Sensitivity	Selectivity	Stability	Reproducibility	Refs.
AuNPs@CNO	GCE	Environmentalpollutanthydrazine	$K_3[Fe(CN)_6]$/ $K_4[Fe(CN)_6]$	Differential pulse voltammetry (DPV) and amperometry (applied potential of + 0.90 V)	12 nM	0.05-1000 μM	485.7 μA/ mM cm^{-2}	Inorganic ions,Atr, H_2O_2, RS, Oxalic acid and Ur	5 days (relative standard error is 1.5 %)	3 independent electrodes (relative error: 1.78 %)	[42]
CNO/ MoS2/ Ag dendrites	SPCE	EPi	1 mM $K_3[Fe(CN)_6]$/ $K_4[Fe(CN)_6]$	CV and EIS	0.03 nM	0.1–500 nM	–	Methotrexate, fluorouracil, and daunorubicin	–	3 independent electrodes (relative standard deviation of 2.54 %)	[74]
AgNDs/ CNOs	GCE	Methamphetamine	5 mM $K_3[Fe(CN)_6]$/ $K_4[Fe(CN)_6]$	CV, DPV, and EIS	30 nM	0.099–59.88 μM	–	Codeine (COD), Diclofenac, ACT, Methimazole, UA, EP, Glu, Gly, Cysteine (Cys)-and AA	1 month	4 independent electrodes (relative standard deviation of 2.7 %)	[82]
Pt@CNO/Nafion	GC	Glucose	0.01 M PBS (pH = 7.4)	CV (100 mV/s) and hydrodynamic amperometry (potential of 0.45 V)	0.09 mM	1–10 mM	21.6 μA/ mM cm^{-2}	–	Three consecutive calibrations tests	–	[72]
AuNPs/ CNOs/ SWCNTs/CS	GCE	Carcinoembryonic antigen (CEA)	$[Fe(CN)_6]^{3/4-}$	SWV	100 fg mL^{-1}	100 fg mL^{-1} to 400 ng mL^{-1}	High sensitivity	Cortisol (Cor), DHEA, Alphafeto protein (AFP), Leptin, AA, Haptoglobin, BSA, UA, hCG, and a cocktail of antigens	28 days (efficiency of 84 %)	Five different electrodes	[93]
CNOs	GCE	Methylene blue	0.1 M HCl	SWV	64.23 pM	100–1000 pM	-	Different cations and anions	–	–	[73]
AuNP/NCNO	GCE	Acetaminophen	0.1 M PBS containing 5 mM $K_3Fe(CN_6)/K_4Fe(CN_6)$ and 0.1 M KCl	CV (form 0.01 to 0.30 V·s^{-1})	9 nM	25 nM–0.1 μM	–	AA, DA, CA, L-cysteine, glucose, H_2O_2, iron, nitrate, chloride, and fructose	4 weeks (3.98 % signal decrease)	Four different electrodes were employed, and the RSD was 2.94 %	[39]
Au/Apt/ox-CNOs/MB	Au/Apt	Epirubicin	1 mM $K_3Fe(CN_6)$/ $K_4Fe(CN_6)$	CV (potential range of −0.4 to 0.4 V)	0.33 nM	1–75 nM	0.36 μl/nM	Daunorubicin, methotrexate, and toremifene	–	Four electrochemical aptasensors (RSD of 2.34 %)	[37]
CNOs	GCE	Simultaneous detection of dopamine, uric acid, L-tryptophan, and theophylline	0.1 M PBS	DPV(Scan rate: 50 mV/s)	0.0039 μM, 0.0087 μM, 0.18 μM, 0.35 μM, respectively.	0.01–38.16 μM (DA) 0.06–68.16 μM (UA) 1.00–108.25 μM (Trp) 8.16–108.25 μM (TP)	High sensitivity	Inorganic ions, Gly, L-lysine, L-valine, Ad, and AA	30 days (the current response was 91.56 %, 95.84 %, 93.91 % and 93.24 %, respectively)	6 electrodes (RSD of DA, UA, Trp, and TP were 3.82 %, 3.67 %, 4.16 %, and 3.10 %, respectively)	[77]

Table 7. continued

System	Electrodes	Target analyte	Electrolyte	Detection method	Detection limit	Linear Range	Sensitivity	Selectivity	Stability	Reproducibility	Refs.
ZnO/CNO	GCE	Glucose	0.1 M NaOH	CV (−1.6 to + 1.6 V)	0.1 mM	1–15 mM	606.64 μA/mM cm^2	AA, CA, LA, ethanol, glycerol, urea	40 days (shows a decrease from 700 to 430 μA)	–	[78]
CNOs	SCL (optic)	Ovariancancerbiomarker	–	–	3.3 fg/mL	10^{-5}–10 ng mL^{-1}	–	HPV16 (E6) protein, human interleukin-6 (IL-6), and the lipolysis-stimulated lipoprotein receptor (LSR)	–	Six repetitions of the immune recognition process (RSD were 2.55 and 2.40 %)	[80]
Pd/CNOs	GCE	Dopamine	0.1 M PBS	CV (Scan rate of 25 mV/s)	2.44 μM	10–400 μM	1.93 μA/μM cm^2	AA, UA, Glu, and H_2O_2	22 days (2.48 ± 0.28 and 2.52 ± 0.57 for the 1st and 22nd days respective)	Three different sensors (RSD of 3.06 %)	[69]
GNPs/CNOs/CS	GCE	Thrombin	5 mM$[Fe(CN)_6]^{3/4-}$	CV (Scan rates: 20 to 100 mV/s)	8.61 fM	26.74 pM–26.74 fM	–	Apolipoprotein A1 (ApoA1), C-reactive protein (CRP), Vascular endothelial growth factor (VEGF), Lipocalin-2 (LCN2) and Leptin	14 days (retained the electrochemical response at 92 % of its original signal)	–	[54]
N-CNO	GC	Dihydroxybenzenes isomers: HQ, CC, RS	$[Fe(CN)_6]^{3/4-}$	CV at 50 mV/s DPV was used for their simultaneous determination	0.49 nM, 0.13 nM, 7.30 nM, respectively	100 nM–1 mM	645 μA/μM cm^2, 1069 μA/μM cm^2, 1191 μA/μM cm^2, respectively.	–	2 weeks (the response for HQ, CC, and RS remained at 96, 95 and 91 %)	15 repeated measurements of the three independent electrodes exhibited an RSD of 3.5 %	[72]

Table 8. Biosensing applications of different carbon nanostructures.

Electrodes	Carbon nanomaterial	Target	Limit of Detection	Selectivity (Interferents)	Stability	Linear Range	Real samples Analysis	Ref.
Diamond-based sensors								
SPCE	diamond nanoparticles	Anti-cancer drug flutamide	0.023 μM	Caffeine, Glu, UA, $MgCl_2$, and $FeCl_2$.	25 days	0.025–606.65 μM	Yes	[96]
SPE	Tyr/PLL/ND- IL	CC	1.1×10^{-8} M	Glu, AA, Ur, UA, Et, Methanol, 1-naphthol, 2-naphthol, Mg^{2+}, Ca^{2+}, K^+, Cl^- and NO_3^-	25 days	5.0×10^{-8}–1.2×10^{-5} M	Yes	[97]
CNTs-based sensors								
SPCE	PPy-NTs and MWCNT-COOH	HopQprotein	2.06 pg/mL	Glu, AA, BSA, and DA	–	5 pg/mL–1.063 ng/mL	Yes	[98]
GCE	B and N co-doped CNTs	Uric acid	0.078 μM and 4.52 μM	–	–	2–400 μM And 5–200 μM	Yes	[99]
TFT	CNT-array	SARS-CoV-2 S1 protein	6 aM (3.6 copies/μL)	SARS-CoV S1 protein (500 nM) and MERS-CoV S1 protein	79 days	1 fM–500 nM	No	[100]
GCE	MWCNT-SB-dBA nanohybrid	H_2O_2	58 nM	–	14 days	0,175 μM–6,12 μM	Yes	[101]
–	cGQDs-functionalized CNTs	Endotoxin	4.6 fg/mL	Glycans, AminA, and ATP	7 days	100 fg/mL-1 ng/mL	Yes	[102]
–	MCTA-MWCNT-FET	Microcystin-LR	0.11 ng/mL	MC-YR and MC-LY	60 days	0.1–0.5 ng/mL	Yes	[103]
PGE	MWCNTs/pPy	UA	0.76 mM	DA, L-AA, CA, NaCl, KCl, sarcosine, and Glu	19 days	0.22–3.5 mM	No	[104]
GCE	Laccase-Based-MWCNTs	Catechol And hydroquinone	0.028 μM and 0.15 μM	Mg^{2+}, Ca^{2+}, Zn^{2+}, Cu^{2+}, Fe^{2+}, Cl^-, NO_3^-, and SO_4^{2-}, 50-fold Et, Glu, AA, PhOH and nitrophenol	–	0.1–57 μM and 0.5–57 μM	No	[92]
Graphene-based sensors								
LSG	Laser-scribing graphene-based	AFP and CEA	13.68 pg mL^{-1} and 50.66 pg mL^{-1}	BSA, IgG, PSA, NSE, AFPand CEA	25 days	0.75 ng/mL–100 ng/mL	No	[105]
–	Au-functionalized wrinkle graphene	Interleukin-6	33.6 fg/mL	IL-2 and IL-10	–	Not Reported	Yes	[106]
–	Graphene Oxide Nanosheets	Lactate	1 mM	Cor	–	1.3–113.4 mM	Yes	[107]
–	CS-modified graphene field transistor	Procalcitonin	0.82 ag/mL	Interleukin-6, C-reactive protein (CRP), and their mixture	–	1ag/mL-10 pg/mL	Yes	[108]
–	planar-gated graphene field-effect transistor	Circulating tumor cells	1 cell/15 μl(~66/ml)	U937 cells	–	1 cell/15 μl–1 cell/1000 μl	No	[109]
CDs-based sensors								
Nano-biosensor	MnO_2 NSs- BCDs	*Staphylococcusaureus*	9CFU/mL and 22 CFU/mL	L. monocytogenes, E. coli O157:H7, V.parahaemolyticus and their mixtures	–	37–3.7×10^6 CFU/mL	Yes	[110]
–	Carbon dot-copper nanocomposite	Creatinine	5.1×10^{-16} mg dL^{-1}	Glu, Ur, and AA	3 months	10^{-5}–0.1 mg dL^{-1}	Yes	[111]
–	BC-CDs-Cu	tert-butylhydroquinone	70 nM	Metal ions, anions, or reducing agents	–	0.5–20.0 μM	Yes	[112]
–	OCDs@$^{PSA}Ab_{HRP}$	PSA	38 pg ml^{-1} and 55 pg ml^{-1}	AFP, CEA, Common proteins, AminA, UA, and AA	Less than a 4% decrease after 100 cycles	0.1–100 ng ml^{-1} and 5–120 ng ml^{-1}	Yes	[113]
–	red-emitting carbon dots and green-emitting CDs	*C. jejuniand* A.butzleri	1 CFU/mL	A. butzleriand *C.jejuni*	Not Reported	0–1×10^7 CFU/mL	Yes	[114]
–	β-cyclodextrin – phenylboronic acid-CDs	α-glucosidase	0.030 U/L	Amino acids, proteins, and natural enzymes	4 months	5.00–150 μmol/L	No	[115]

7.3. Stability

The sensing properties of CNO-based electroanalytical sensors vary over time due to continuous operation. In practical terms, a system's capacity for extended use or repeated cycles primarily hinges on its stability. CNO-based biosensing devices exhibit good durability. Several studies, such as the one by An *et al*.,[77] not only designed a biosensor capable of detecting and differentiating low biomolecule concentrations (dopamine, uric acid, L-tryptophan, and theophylline) but also maintaining 90% of the initial efficiency within 30 days of usage. This could be attributed to the structural stability of the CNOs with their concentric layers and their resistance to physicochemical degradation. These properties are also exhibited by other carbon nanomaterials and devices capable of retaining electrochemical properties for several days. However, CNTs stand out first in this aspect,[100, 103] followed by different materials such as graphene,[105] nanodiamonds,[96–97] and CDs,[115] all showing good durability.

8. Conclusions

Our literature analysis has shown that CNOs are excellent supports for the functionalization of multiple inorganic materials, which ensures outstanding performance for electrochemical sensing and biosensing. Indeed, such devices have displayed low detection limits, wide linear detection ranges, remarkable selectivity, reproducibility, and stability. The review explored different synthetic methods and essential characterization techniques for these nanostructures, highlighting the crucial role and promising potential of CNOs in the field of electroanalytical chemistry. A comparison with other carbon materials underscored the competitive advantage of CNOs despite their relatively recent introduction within the biosensing field.

Despite the fact that CNOs have been known for decades and the manifest interest of the scientific community in their properties and reactivity, there are significant gaps in the comprehension of their structure-reactivity relations. By far, other carbon nanomaterials such as graphene, carbon nanotubes, or fullerenes have been more studied than CNOs by experimental and theoretical means. Considering the case of CNOs, it remains a fundamental question whether the effect of holes, strain, or the differential reactivity of hexagons, pentagons, and heptagons follows the same trend as in other carbon-based nanomaterials. Likewise, the effect of defects on reactivity has been addressed in the framework of electrocatalysis, with emphasis on energy applications and the oxygen reduction reaction. Instead, the electro-bio-analytical field has a large variety of target molecules (as depicted in Tables 7 and 8) and therefore the specific information regarding the actual role of the active sites at the surface of CNOs is missing so far. We believe that further directions in research to establish the fate of reactive intermediates at the surface of CNOs should be driven toward operando Spectro electrochemistry, where vibrational spectroscopy coupled with Hessian computations[116] would be instrumental in establishing the identity of key intermediates and the specific reaction pathways under different reaction conditions (supporting electrolyte, solvent, pH, ionic strength). Such an understanding would be essential for the design of electroanalytical biosensors with improved selectivity and response time since eventual bottlenecks in the reaction mechanisms associated with analyte transformation could be detected and solved via the adequate modification of the electrode | electrolyte interface.

Such understanding will open the door for the design of more sensitive and specific electrochemical sensors where CNOs would play an outstanding role. Future perspectives aimed to push the boundaries of detection limits and enhance selectivity, reproducibility, and stability through the exploration of novel synthesis approaches and alternative functionalization of CNOs. The synergistic effect achieved by the combination of CNOs with other carbon nanostructures has raised particular interest in electrochemical applications, offering new pathways for improved sensor performance, thus offering a path for enhanced sensor performance in the future.

Acknowledgments

The work was funded by the European Union (Marie Skłodowska Curie Postdoctoral Fellowship, PROTO-BACT, 101107715; ERC Starting Grant, PROTOMAT, 101039578). Views and opinions expressed are, however, those of the authors only and do not necessarily reflect those of the European Union or the European Research Council. Neither the European Union nor the granting authority can be held responsible for them. Open Access publishing facilitated by Università degli Studi di Trieste, as part of the Wiley - CRUI-CARE agreement. Open Access publishing facilitated by Università degli Studi di Trieste, as part of the Wiley - CRUI-CARE agreement.

Conflict of Interests

The authors declare no conflict of interest.

Keywords: carbon nano-onions · biosensing · biosensors · carbon nanostructures · electroanalysis · sensing.

[1] S. Iijima, *J. Cryst. Growth* **1980**, *50* (3), 675–683.
[2] M. Terrones, G. Terrones, H. Terrones, *Struct. Chem.* **2002**, *13* (3), 373–384.
[3] S. Jung, Y. Myung, G. S. Das, A. Bhatnagar, J.-W. Park, K. M. Tripathi, T. Kim, *New J. Chem.* **2020**, *44 (18)*, 7369–7375.
[4] A. Camisasca, S. Giordani, *Carbon Nano-onions for Bioimaging and Cancer Therapy Applications, in Nanooncology: Engineering nanomaterials for cancer therapy and diagnosis* (eds.Gonçalves, G., Tobias, G.), Springer International Publishing, Cham, **2018**, pp. 417–455.
[5] G. Centi, K. Barbera, S. Perathoner, N. K. Gupta, E. E. Ember, J. A. Lercher, *ChemCatChem* **2015**, *7* (18), 3036–3046.
[6] G. Wu, M. Nelson, S. Ma, H. Meng, G. Cui, P. K. Shen, *Carbon* **2011**, *49* (12), 3972–3982.
[7] A. Singh, A. Sharma, A. Ahmed, A. K. Sundramoorthy, H. Furukawa, S. Arya, A. Khosla, *Biosensors* **2021**, *11* (9), 336.
[8] Y. Liu, R. L. Vander Wal, V. N. Khabashesku, *Chem. Mater.* **2007**, *19* (4), 778–786.

[9] D. Ugarte, *Nature* **1992**, *359*, 707–709.
[10] Z. Lin, G. Shao, W. Liu, Y. Wang, H. Wang, H. Wang, B. Fan, H. Lu, H. Xu, R. Zhang, *Carbon* **2022**, *192*, 356–365.
[11] F. Banhart, *Trans. R. Soc.* **2004**, *(362)*, 2205.
[12] A. V. Krasheninnikov, F. Banhart, *Nat. Mater.* **2007**, *6* (10), 723–733.
[13] A. Palkar, F. Melin, C. Cardona, B. Elliott, A. Naskar, D. Edie, A. Kumbhar, L. Echegoyen, *Chem. Asian J.* **2007**, *2*, 625–633.
[14] O. Mykhailiv, A. Lapinski, A. Molina-Ontoria, E. Regulska, L. Echegoyen, A. T. Dubis, M. E. Plonska-Brzezinska, *ChemPhysChem* **2015**, *16* (10), 2182–2191.
[15] C. T. Cioffi, A. Palkar, F. Melin, A. Kumbhar, L. Echegoyen, M. Melle-Franco, F. Zerbetto, G. M. A. Rahman, C. Ehli, V. Sgobba, D. M. Guldi, M. Prato, *Chem. Eur. J.* **2009**, *15* (17), 4419–4427.
[16] Y. Gan, F. Banhart, *Adv. Mater.* **2008**, *20* (24), 4751–4754.
[17] M.-J. Xiao, B. Ma, Z.-Q. Zhang, Q. Xiao, X.-Y. Li, Z.-T. Zhang, Q. Wang, Y. Peng, H.-L. Zhang, *J. Mater. Chem. A* **2021**, *9* (11), 7227–7237.
[18] C. Zhang, J. Li, C. Shi, C. He, E. Liu, N. Zhao, *J. Energy Chem.* **2014**, *23* (3), 324–330.
[19] Y. Liang, A. Gu, S. Wang, Y. He, S. Zheng, J. Guo, F. S. Boi, *CrystEngComm* **2023**, *25* (38), 5382–5386.
[20] J. Yang, Y. Zhang, D. Y. Kim, *Carbon* **2016**, *98*, 72–82.
[21] M. Ghasemlou, N. Pn, K. Alexander, A. Zavabeti, P. C. Sherrell, E. P. Ivanova, B. Adhikari, M. Naebe, S. K. Bhargava, *Adv. Mater.* **2024**, *36* (19), 2312474.
[22] X. Gan, H. Zhao, *Sens. Mater.* **2015**, *27*, 191–215.
[23] M. Zeiger, N. Jäckel, V. N. Mochalin, V. Presser, *J. Mater. Chem. A* **2016**, *4* (9), 3172–3196.
[24] S. Sang, S. Yang, A. Guo, X. Gao, Y. Wang, C. Zhang, F. Cui, X. Yang, *Chem. Asian J.* **2020**, *15* (21), 3428–3431.
[25] W. Liu, Y. Miao, Q. Meng, *Integr. Ferroelectr.* **2012**, *138*, 77–82.
[26] L. Hernandez-Tabares, J. G. Darias-Gonzalez, F. J. Chao-Mujica, L. M. Ledo-Pereda, M. Antuch, E. Carrillo-Barroso, J. E. Chong-Quero, E. Reguera, L. F. Desdin-Garcia, *J. Nanomater.* **2021**, 12.
[27] L. Hernandez-Tabares, F. J. Chao-Mujica, J. G. Darias-Gonzalez, L. M. Ledo Pereda, M. Antuch, E. Carrillo-Barroso, J. E. Chong-Quero, L. F. Desdin-Garcia, *J. Nanomater.* **2024**, *2024*, 9949667.
[28] I. Padron-Ramirez, N. Torres-Figueredo, A. L. Corcho-Valdes, J. P. de Leon-Cabrera, F. J. Chao-Mujica, K. V. Cruz, M. Antuch, J. Deschamps, E. Reguera, L. F. Desdin-Garcia, *Adsorption* **2023**, *30*, 25–28.
[29] F. J. Chao-Mujica, A. L. Corcho-Valdes, I. Padron-Ramirez, J. P. de Leon - Cabrera, L. Hernandez-Tabares, M. Antuch, L. F. Desdin-Garcia, *Adv. Nat. Sci. Nanosci. Nanotechnol.* **2024**, *15* (1), 015016.
[30] L. García, F. Chao-Mujica, L. Hernandez-Tabares, L. Hernández, J. Darias, L. Ledo, A. L. Corcho-Valdés, M. Antuch, *Progresos en la síntesis de nanoestructuras de carbono por descarga de arco sumergida.* **2023**, *73*, 25–28.
[31] N. Sano, H. Wang, I. Alexandrou, M. Chhowalla, K. B. K. Teo, *J. Appl. Phys.* **2002**, *92* (5).
[32] R. Borgohain, J. Yang, J. P. Selegue, D. Y. Kim, *Carbon* **2014**, *66*, 272–284.
[33] J. C. Zuaznabar-Gardona, A. Fragoso, *Electrochim. Acta* **2020**, *353*, 136495.
[34] J. J. Ogada, T. J. Ehirim, A. K. Ipadeola, A. B. Haruna, P. V. Mwonga, A. M. Abdullah, X.-Y. Yang, K. Eid, D. M. Wamwangi, K. I. Ozoemena, *ACS Omega* **2024**, *9* (7), 7439–7451.
[35] Y. Guo, H. Lu, X. jian, *Ceram. Int.* **2024**, *50* (5), 8030–8041.
[36] A. B. Hashkavayi, J. B. Raoof, *Biosens. Bioelectron.* **2017**, *91*, 650–657.
[37] E. Sohouli, M. Ghalkhani, T. Zargar, F. Ahmadi, *Biosensors* **2022**, *12* (12), 1339.
[38] V. Sok, A. Fragoso, *Appl. Sci.* **2021**, *11* (15), 6889.
[39] E. Sohouli, F. Shahdost-Fard, M. Rahimi-Nasrabadi, M. Plonska-Brzezinska, F. Ahmadi, *J. Electroanal. Chem.* **2020**, *871*, 114309.
[40] V. Dhand, J. S. Prasad, M. V. Rao, S. Bharadwaj, Y. Anjaneyulu, P. K. Jain, *Mater. Sci. Eng. C* **2013**, *33*, 758–762.
[41] E. Murphy, S. K. Guin, A. Lapiy, A. Camisasca, S. Giordani, E. Dempsey, *Electrochem. Sci. Advances* **2024**,, e2300027.
[42] N. S. K. Gowthaman, D. Mohapatra, P. Arul, W. S. Chang, *J. Ind. Eng. Chem.* **2023**, *117*, 227–237.
[43] A. Panda, S. K. Arumugasamy, J. Lee, Y. Son, K. Yun, S. Venkateswarlu, M. Yoon, *Appl. Surf. Sci.* **2020**, *537*, 147872.
[44] A. Guo, K. Bao, S. Sang, X. Zhang, B. Shao, C. Zhang, Y. Wang, F. Cui, X. Yang, *RSC Adv.* **2021**, *11* (12), 6850–6858.
[45] C. Zhai, X. Kong, K. Hu, L. Wang, X. Fan, *Chem. Phys. Lett.* **2019**, *738*, 136866.
[46] M. E. Plonska-Brzezinska, A. Lapinski, A. Z. Wilczewska, A. T. Dubis, A. Villalta-Cerdas, K. Winkler, L. Echegoyen, *Carbon* **2011**, *49* (15), 5079–5089.
[47] L. Hawelek, A. Brodka, S. Tomita, J. C. Dore, V. Honkimäki, A. Burian, *Diamond Relat. Mater.* **2011**, *20* (10), 1333–1339.
[48] G. Ostroumova, N. Orekhov, V. Stegailov, *Diamond Relat. Mater.* **2019**, **94**, 14–20.
[49] J. Goclon, *Appl. Surf. Sci.* **2020**, *532*, 147267.
[50] J. Goclon, B. Bankiewicz, P. Kolek, K. Winkler, *Carbon* **2021**, **176**, 198–208.
[51] M. A. Hashmi, M. Lein, *J. Phys. Chem. C* **2018**, *122* (4), 2422–2431.
[52] C. Zhang, H. Du, K. Ma, Z. Yuan, *Adv. Energy Mater.* **2020**, *10* (43), 2002132.
[53] O. Mykhailiv, M. Imierska, M. Petelczyc, L. Echegoyen, M. E. Plonska-Brzezinska, *Chem. Eur. J.* **2015**, *21* (15), 5783–5793.
[54] M. Afaque Ansari, W. Juen Liew, C. Padmakumari Kurup, M. U. Ahmed, *J. Electroanal. Chem.* **2023**, *937*, 117422.
[55] D. Pech, M. Brunet, H. Durou, P. Huang, V. Mochalin, Y. Gogotsi, P.-L. Taberna, P. Simon, *Nat. Nanotechnol.* **2010**, *5* (9), 651–654.
[56] D. M. Bobrowska, E. Castro, L. Echegoyen, M. E. Plonska-Brzezinska, *ChemNanoMat* **2020**, *6* (2), 248–257.
[57] J. Breczko, M. E. Plonska-Brzezinska, L. Echegoyen, *Electrochim. Acta* **2012**, *72*, 61–67.
[58] J. Breczko, M. Wysocka-Żołopa, E. Grądzka, K. Winkler, *ChemElectroChem* **2024**, *11* (10), e202300752.
[59] G. S. Das, R. Panigrahi, S. Ghosh, K. M. Tripathi, *Mater. Today Sustain.* **2024**, *25*, 100656.
[60] X. Peng, Y. Li, F. Kang, X. Li, Z. Zheng, L. Dong, *Small* **2024**, *20* (4), 2305547.
[61] M. Plonska-Brzezinska, *ChemNanoMat* **2019**, *5*, 568–580.
[62] K. Guo, Z. He, S. Lu, P. Zhang, N. Li, L. Bao, Z. Yu, L. Song, X. Lu, *Adv. Funct. Mater.* **2023**, *33* (29), 2302100.
[63] J. Adhikari, M. Rizwan, N. A. Keasberry, M. U. Ahmed, *J. Chin. Chem. Soc.* **2020**, *67* (6), 937–960.
[64] N. Baig, A.-N. Kawde, M. Ibrahim, *Mater Adv* **2020**, *1* (4), 783–793.
[65] Z. Abdul Rahim, N. A. Yusof, M. A. S. Mohammad Haniff, F. Mohammad, M. I. Syono, N. Daud, *Materials* **2018**, *11* (10).
[66] B. Shaku, T. P. Mofokeng, T. H. Mongwe, N. J. Coville, K. I. Ozoemena, M. S. Maubane-Nkadimeng, *Electroanalysis* **2020**, *32* (12), 2946–2957.
[67] D. Mohapatra, M. S. Sayed, J.-J. Shim, *Nanomaterials* **2023**, *13* (1).
[68] D. Codorniu-Pujals, D. R. Garcés, O. A. de Fuentes, L. F. D. García, *Nucleus* **2018**, 64.
[69] H. H. Ipekcı, *Hittite J. Sci. Eng.* **2023**, *10* (3), 201–209.
[70] L. R. Cumba, A. Camisasca, S. Giordani, R. J. Forster, *Molecules* **2020**, *25* (17), 3884.
[71] M. Bartkowski, V. Bincoletto, I. C. Salaroglio, G. Ceccone, R. Arenal, S. Nervo, B. Rolando, C. Riganti, S. Arpicco, S. Giordani, *J. Colloid Interface Sci.* **2024**, *659*, 339–354.
[72] J. Mohapatra, B. Ananthoju, V. Nair, A. Mitra, D. Bahadur, N. V. Medhekar, M. Aslam, *Appl. Surf. Sci.* **2018**, *442*, 332–341.
[73] A. V. Ramya, R. Thomas, M. Balachandran, *Ultrason. Sonochem.* **2021**, *79*, 105767.
[74] H. Teymourinia, L. Sánchez, F. Mollaie, M. Ghalkhani, A. Ramazani, L. V. Hublikar, T. M. Aminabhavi, *Chem. Eng. J.* **2024**, *480*, 148307.
[75] V. Thapliyal, M. E. Alabdulkarim, D. R. Whelan, B. Mainali, J. L. Maxwell, *Diamond Relat. Mater.* **2022**, *127*, 109180.
[76] P. Olejnik, M. Gniadek, L. Echegoyen, M. E. Plonska-Brzezinska, *Electroanalysis* **2021**, *33* (4), 1107–1114.
[77] R. An, W. Kuang, Z. Li, T. Mu, H. Luo, *Processes* **2023**, *11* (9), 2547.
[78] A. Sharma, A. Agrawal, G. Pandey, S. Kumar, K. Awasthi, A. Awasthi, *ACS Omega* **2022**, *7* (42), 37748–37756.
[79] V. Singh, *Diamond Relat. Mater.* **2018**, *87*, 202–207.
[80] Y. Huang, S. Zhang, Y. Chen, L. Gao, H. Dai, Y. Lin, *J. Mater. Chem. B* **2023**, *11* (30), 7209–7216.
[81] S. G. Yastrebov, V. I. Ivanov-Omskii, *Semiconductors* **2007**, *41* (12), 1430–1433.
[82] Z. Khorablou, F. Shahdost-Fard, H. Razmi, *Surf. Interfaces* **2022**, *31*, 102061.
[83] N. Elgrishi, K. J. Rountree, B. D. McCarthy, E. S. Rountree, T. T. Eisenhart, J. L. Dempsey, *J. Chem. Educ.* **2018**, *95* (2), 197–206.
[84] M. Antuch, A. Ranjbari, S. A. Grigoriev, J. Al-Cheikh, A. Villagrá, L. Assaud, Y. Z. Voloshin, P. Millet, *Electrochim. Acta* **2017**, *245*, 1065–1074.
[85] O. C. Ozoemena, L. J. Shai, T. Maphumulo, K. I. Ozoemena, *Electrocatalysis* **2019**, *10* (4), 381–391.

[86] H. S. Magar, R. Y. A. Hassan, A. Mulchandani, *Sensors* **2021**, *21* (19), 6578.
[87] S. Wang, J. Zhang, O. Gharbi, V. Vivier, M. Gao, M. Orazem, *Nat. Rev. Methods Primers* **2021**, *1*, 41.
[88] K. Čerņevičs, M. Fuechsle, M. Broome, M. Choucair, O. V. Yazyev, *Carbon* **2023**, *208*, 303–310.
[89] J. Zhu, Y. Huang, W. Mei, C. Zhao, C. Zhang, J. Zhang, I. S. Amiinu, S. Mu, *Angew. Chem. Int. Ed.* **2019**, *58* (12), 3859–3864.
[90] *T. Yu. Astakhova, G. A. Vinogradov, O. D. Gurin, M. Menob, Russ. Chemical Bull.* **2002**, *51 (5)*, 764–769.
[91] S. P. Zankowski, P. M. Vereecken, *ACS Appl. Mater. Interfaces* **2018**, *10* (51), 44634–44644.
[92] S. Malinowski, M. Wardak, C. Wardak, *Langmuir* **2024**, 2942.
[93] M. Rizwan, S. Elma, S. A. Lim, M. U. Ahmed, *Biosens. Bioelectron.* **2018**, *107*, 211–217.
[94] C. Iriarte-Mesa, Y. López, Y. Matos-Peralta, K. de la Vega-Hernández, M. Antuch, Top. Curr. Chem. (Z), **2020**, 378, 12.
[95] A. L. Corcho-Valdés, C. Iriarte-Mesa, J. Calzadilla-Maya, Y. Matos-Peralta, L. Desdín-García, M. Antuch, *Carbon Nanotubes in Organic Catalysis*, In: Jawaid, M., Khan, A. (eds) Carbon Composite Catalysts. Composites Science and Technology, Springer, Singapore, **2022**, pp. 223–266.
[96] N. Baskaran, S. Ballur Prasanna, Y. C. Lin, Y.-F. Duann, R.-J. Chung, Y. Wei, *Sensors* **2024**, *24*, 985.
[97] D. Şener, P. E. Erden, C. Kaçar Selvi, *Anal. Biochem.* **2024**, *688*, 115464.
[98] H. Jaradat, B. M. Hryniewicz, I. A. Pašti, T. L. Valério, A. Al-Hamry, L. F. Marchesi, M. Vidotti, O. Kanoun, *Biosens. Bioelectron.* **2024**, *249*, 115937.
[99] Y. Liu, X. Yan, Y. Xing, P. Zhao, M. Liu, Y. Zhu, L. Li, N. Liu, Z. Zhang, *Microchem. J.* **2024**, *197*, 109770.
[100] S. Ma, Q. Ren, L. Jiang, Z. Liu, Y. Zhu, Z. Jiahao, Y. Zhang, M. Zhang, *Talanta* **2024**, *266*, 124973.
[101] A. Tamborelli, M. López Mujica, O. A. Sánchez-Velasco, C. Hormazábal-Campos, E. G. Pérez, M. Gutierrez-Cutiño, D. Venegas-Yazigi, P. Dalmasso, G. Rivas, P. Hermosilla-Ibáñez, *Talanta* **2024**, *270*, 125520.
[102] Q. Cui, J. Li, Y. Li, L. Tang, K. Li, T. Li, X. Chen, Z. Zhang, G. J. Zhang, *Talanta* **2024**, *266*, 125035.
[103] M. Lee, S. Kim, D. Kim, H. J. Kim, *Biosensors* **2024**, *14*, 37.
[104] E. S. Yulianti, S. F. Rahman, M. Rizkinia, A. Zakiyuddin, *Arab. J. Chem.* **2024**, *17* (4), 105692.
[105] Y.-K. Yen, G.-W. Huang, R. Shanmugam, *Talanta* **2024**, *266*, 125096.
[106] C. Dou, Z. Wu, W. Chen, H. Yan, D. Li, X. Q. You, Y. S. Chen, C. Zhou, S. Chen, P. Zhuang, J. Liu, *Carbon* **2024**, *216*, 118556.
[107] S. Deng, *Alexandria Eng. J.* **2024**, *88*, 31–35.
[108] F. Chen, Y. Zhang, M. Wang, J. Liu, H. Wenfeng, Y. Liu, *Talanta* **2023**, *268*, 125308.
[109] T.-L. Lee, S.-C. Huang, C.-C. Huang, S.-W. Lee, C.-H. Huang, M.-Y. Lan, C.-Y. Su, *Carbon* **2023**, *216*, 118576.
[110] X. Gao, H. Zhang, L. Liu, M. Jia, X. Li, J. Li, *Food Chem.* **2024**, *432*, 137144.
[111] P. Bhatt, D. Kukkar, A. K. Yadav, K. H. Kim, *Spectrochim. Acta Part A* **2024**, *307*, 123666.
[112] W. Fan, L. Guo, Y. Qu, Q. Zhuang, Y. Wang, *J. Hazard. Mater.* **2024**, *468*, 133795.
[113] J. Korram, A. C. Anbalagan, A. Banerjee, S. N. Sawant, *J. Mater. Chem. B* **2024**, *12* (3), 742–751.
[114] L. Weixing, Z. Chengrui, G. Shaoqian, M. Keran, Z. Shangxian, D. Qingbao, S. Kangmin, L. Chenguang, C. Zhe, *Talanta* **2023**, *1* (266), 125085.
[115] M. Liang, G. Song, Y. Wan, Y. Chen, F. Wang, X. Liu, *Chin. Chem. Lett.* **2023**, 3905–3912.
[116] A. L. Corcho-Valdes, J. Ponce de Leon-Cabrera, I. Padron-Ramirez, F. J. Chao-Mujica, E. Lebed, A. Gutierrez-Quintanilla, L. F. Desdin-Garcia, Y. Voloshin, M. Antuch, *J. Phys. Chem. A* **2023**, *127* (45), 9419–9429.

Manuscript received: April 15, 2024
Revised manuscript received: July 30, 2024
Accepted manuscript online: August 14, 2024
Version of record online: ■■, ■■